Coordination Chemistry Reviews 255 (2011) 186–202

Contents lists available at ScienceDirect

Coordination Chemistry Reviews

journal homepage: www.elsevier.com/locate/ccr

Review

# Enzymes with an heterodinuclear iron–manganese active site: Curiosity or necessity?

Michaël Carboni[a,b,c], Jean-Marc Latour[a,b,c,*]

[a] iRTSV/LCBM/pmb, 38054 Grenoble Cedex 09, France
[b] CNRS, UMR 5249, Grenoble, France
[c] Université Joseph Fourier, Grenoble, France

**Contents**



ARTICLE INFO

*Article history:*
Received 7 June 2010
Accepted 5 August 2010
Available online 17 August 2010

*Keywords:*
Purple acid phosphatase
Ribonucleotide reductase

ABSTRACT

This review analyzes the currently available data on true and purported FeMn enzymes with a particular emphasis on their specific physical properties. The characterization of the purple acid phosphatase from *sweet potato* and the current view of the hydrolysis mechanism are presented. The controversy associated with the discovery of the class Ic ribonucleotide reductase from *Chlamydia trachomatis* is discussed in the light of its extensive reactivity and physical studies. The amine oxygenase AurF is presented also albeit it is not exactly an FeMn enzyme but its case is particularly enlightening of the difficulties in assessing which is the right metal of an enzyme. Then, the very recent emergence of a new class of FeMn oxidases is highlighted. Lastly, examination of potential model compounds reveals the paucity of reported examples

* Corresponding author at: Laboratoire iRTSV/LCBM/pmb, Bâtiment C5, CEA – Grenoble, 17 rue des Martyrs, 38054 Grenoble Cedex 9, France.
Tel.: +33 4 38 78 44 07; fax: +33 4 38 78 34 62.
*E-mail address:* Jean-Marc.Latour@cea.fr (J.-M. Latour).

0010-8545/$ – see front matter 
doi:10.1016/j.ccr.2010.08.003

Amine oxygenase
Bimetallic sites
Fe–Mn center

and therefore the need to develop this area. General considerations on biologically active metals and their substitution in hydrolases and redox active proteins are provided and possible reasons for the choice of the peculiar FeMn active site over the more classical diiron center are considered.



## 1. Introduction

It is generally admitted that about half of all enzymes require a metal ion to function [1] and the emergence of bioinformatic techniques has allowed one to delineate the main features of the metallome [2]. In this context the first row transition metals, i.e. manganese, iron, cobalt, nickel and copper, occupy a critical position, being involved in many essential hydrolytic and/or redox enzymatic systems. In many cases this function is associated with a specific property of the metal ion, i.e. its redox potential, so its replacement by any other metal ion will lead to the loss of the function. As a consequence, delivering the right metal to the right protein is generally an issue of utmost importance [1,3]. It has been shown that the concentration of free $Cu^{2+}$ ion is maintained at an extremely low value [4], and this is probably the case for other metals. It is now recognized that all metal ions are taken charge of by sophisticated sensor, transport and storage systems, that fulfill the requirements of the cells by regulating the availability of the necessary metals and expelling the toxic ones [3].

The duality of iron and manganese is especially interesting. Indeed both metals are of utmost biological importance and possess very similar charges and ionic radii (Table 1). As a consequence, in non-heme enzymes they have highly similar coordination environments, mainly composed of combinations of histidines and aspartates/glutamates. On the other hand, whereas very specific functions are associated with each metal, i.e. $O_2$ production for Mn and $O_2$ transport and reduction for Fe, they fulfill a few common ones. This complex duality is illustrated by comparisons of the recently described Fe- and Mn-dependent homoprotocatechuate 2,3-dioxygenases [5] and of superoxide dismutases (SOD) [6]. The former enzymes have been shown by X-ray crystallography to have identical active site structures whatever the metal involved. Moreover, it was recently shown that a reconstitution of the Fe enzyme with Mn or the reverse gave an enzyme with similar activity [5]. This unsensitivity of the catalyzed reaction to the involved metal has been assigned to the fact that whereas the overall reaction implies $O_2$ activation and electron transfers, the metals do not change oxidation state and operate through their acidic properties only [5].

The situation of the SOD enzymes is more complicated. Indeed, while both Fe- and Mn-SOD have been shown by X-ray crystallography to possess identical active sites, in most cases replacing Fe by Mn in a Fe-SOD (or the reverse) leads to an inactive enzyme. In fact, this substitution preserves the activity only in the so-called cambialistic SOD family, and understanding these differences has been attracting active research for many years [6]. The generally accepted mechanism states that during catalysis the metals shuttle between the oxidation states +II and +III in the superoxide reduction to peroxide and back in the oxidation of superoxide to dioxygen. Of course in this case, the overall reaction is more sensitive to the redox potentials of the metals and to the H-bond network involved in the proton transfers to the active site [6].

**Table 1**
Ionic radii of biologically important first row transition metals (high-spin state).

| Ion | Electronic configuration | Coordinance | Ionic radii |
|---|---|---|---|
| $Mn^{2+}$ | $3d^5$ | 6 | 0.83 |
| $Mn^{3+}$ | $3d^4$ | 6 | 0.645 |
| $Fe^{2+}$ | $3d^6$ | 6 | 0.78 |
| $Fe^{3+}$ | $3d^5$ | 6 | 0.645 |
| $Co^{2+}$ | $3d^7$ | 6 | 0.745 |
| $Co^{3+}$ | $3d^6$ | 6 | 0.61 |
| $Ni^{2+}$ | $3d^8$ | 6 | 0.69 |
| $Cu^{2+}$ | $3d^9$ | 5 | 0.65 |

This Fe/Mn duality leads to an even more complicated situation for dinuclear metal sites. Indeed, in this case apart from the two homonuclear dimetal sites, FeFe and MnMn, a third possibility exists to have an heterodimetal site, FeMn. Structural characterization of numerous diiron [7,8] and dimanganese [9,10] enzymes has shown that they use the same combinations of histidines and aspartates/glutamates to hold the two metals in close proximity (ca. 2.5–4.0 Å, depending on their oxidation states). Controversies have arisen at times concerning the true nature of certain enzyme active sites, especially some purple acid phosphatase, ribonucleotide reductase and arylamine oxygenase. For the former two enzymes, the existence of the heterodimetal site FeMn has been definitely established [11,12], while for the latter it was proposed [13] but experimental evidence gathered afterwards strongly support a diiron active site [14]. The aim of this review is to analyze the currently available data on FeMn enzymes with a particular emphasis on their specific physical properties. In addition the very few available model compounds reported so far will be presented. Finally, possible reasons for the choice of the peculiar heteronuclear active site over the more classical diiron center will be considered.

## 2. The FeMn purple acid phosphatase

### 2.1. Presentation

Purple acid phosphatases (PAP) belong to the large family of dinuclear metallohydrolases that encompasses diverse phosphatases, RNA and DNA polymerases and peptidases to mention a few [15,16]. Metallohydrolases assemble at their active sites various homometallic pairs $Zn_2$, $Ni_2$, $Co_2$, $Fe_2$, $Mn_2$ and $Mg_2$ and even a few heterometallic ones FeZn and FeMn. The PAPs' active site comprises a ferric ion associated with a divalent metal that is $Fe^{II}$ for mammalian enzymes and $Zn^{II}$, $Fe^{II}$ or $Mn^{II}$ for those of plant origin. They owe their name to the fact that their phosphatase activity maximizes at acidic pH and that they exhibit a purple color attributed to a tyrosinate → $Fe^{III}$ charge transfer transition. While the $Fe^{III}$ ion is strongly bound, the $M^{II}$ ion is more labile and can be exchanged easily in uteroferrin without a significant loss of activity [17].

### 2.2. Structural and physical characterization

X-ray structures of PAP enzymes of mammalian [18] and plant [19,20] origins have been reported and reveal a high degree of homology of the active site whatever the metal pair involved $Fe^{III}Fe^{II}$, $Fe^{III}Zn^{II}$ or $Fe^{III}Mn^{II}$. Most plant PAPs are homodimers with a monomer subunit of ~55 kDa. It is common that several PAP isoforms exist within an organism and sweet potato possesses three isoforms with the three types of dimetal centers $Fe^{III}Fe^{II}$, $Fe^{III}Zn^{II}$ or $Fe^{III}Mn^{II}$ [11,21,22]. The presence of $Fe^{III}Mn^{II}$ center in isoform 2 was demonstrated by Schenk et al. [11] and a similar center was reported very recently in diphosphonucleotide phosphatase/phosphodiesterase from yellow lupin [23]. Fig. 1 depicts the structure of the active site of the PAP from sweet potato isoform 2 with a FeMn pair complexed by a phosphate anion [20].

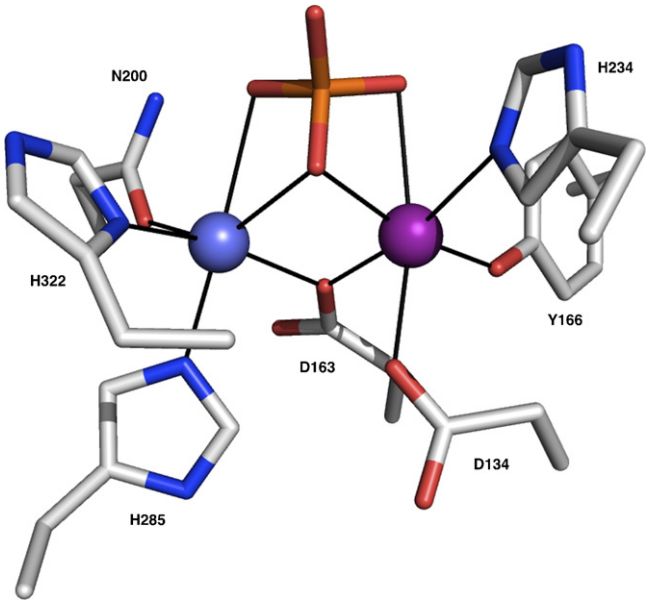


**Fig. 1.** X-ray structure [24] of the binuclear center in the PAP-phosphate complex from sweet potato (PDB code: 1XZW) [20]. The iron and manganese atoms are colored in purple and blue, respectively.

The active site is assembled by seven residues that are strictly conserved in PAPs of all origins (Table 2) while structural differences can exist in other regions of the proteins.

The Fe and Mn ions are hexacoordinated and terminally bound by three residues, Tyr166, His324, Asp134 for Fe and His285, His322, Asn200 for Mn. In addition, the metals are triply bridged by an aspartate (Asp163) and an exogeneous phosphate. The latter is supposed to have displaced an oxygen bridge present in the resting state of the enzyme. This solvent derived bridging ligand was assigned as an oxide from magnetic susceptibility experiments that revealed a very weak magnetic contribution of the enzyme preparation, that is consistent only with a strongly antiferromagnetically coupled Fe–Mn pair ($-2J \gg 140\,cm^{-1}$) [11]. The validity of this assignment was substantiated by recent DFT calculations [25]. As noted by the authors, this is the only example in the literature of a $Fe^{III}$-(μ-O)-$Mn^{II}$ unit [11]. This strong antiferromagnetic coupling differs from those estimated for $Fe^{III}Fe^{II}$ centers in bovine spleen (as-purified) and red kidney bean (reconstituted) PAP by magnetic susceptibility [26] and for uteroferrin by magnetic susceptibility [27], Mössbauer [28] and MCD [29] spectroscopies. Indeed, in the three proteins moderate antiferromagnetic exchange interactions ($-2J \sim 5$–$17\,cm^{-1}$) were estimated. These values are consistent with an hydroxide bridge. In addition, it is well documented that $Mn^{II}$ does not generally give high magnetic exchange interactions owing to its poor covalent bonding. Therefore, the purported $Fe^{III}$-(μ-O)-$Mn^{II}$ unit does not appear fully ascertained yet and additional evidence to support it should be gained from MCD or Mössbauer spectroscopies.

**Table 2**
Metal binding residues in PAPs of various origins.

| |
|---|
| Rat PAP [18] |
| Fe: Tyr55, His223, Asp14, Asp52 |
| Fe: His221, His186, Asn91, Asp52 |
| Red kidney bean PAP [19] |
| Fe: Tyr167, His325, Asp135, Asp164 |
| Zn: His286, His323, Asn201, Asp164 |
| Sweet potato PAP [20] |
| Fe: Tyr166, His324, Asp134, Asp163 |
| Mn: His285, His322, Asn200, Asp163 |

### 2.3. Functional aspects

A common important issue for metallohydrolases, that is a matter of debate, is the identity of the active nucleophile that attacks the substrate phosphorus or equivalent atom. Indeed, while it is generally admitted that the incoming substrate binds at the $M^{II}$ ion by substituting a water molecule, whether it is then attacked (i) by a terminal hydroxide on the $Fe^{III}$ ion or (ii) by a water molecule H-bonded to it or (iii) by the bridging (hydr)oxide has not been firmly established yet. As mentioned above, it was shown in uteroferrin [17] that the enzymatic activity is not much affected by the exchange of the $M^{II}$ metal. This is understandable since the role of this metal is confined to substrate binding. On the other hand, PAPs of different origins or isoforms exhibit different reactivities in terms of catalytic efficiencies and/or pH dependence. It is noteworthy that the FeMn PAP appears the most active, a fact possibly linked to its oxo bridge acting as a nucleophile or to the presence of second-sphere residues favoring the elimination of the leaving group [16]. The latter view is supported by a very recent kinetic study comparing the activities of the FeFe and FeMn forms of uteroferrin that concluded that both forms hydrolyze monoesters through mechanism (ii). Nevertheless, this mechanistic question may not have a unique answer since it was shown earlier that it may depend on substrates (mono vs diesters) [30].

## 3. The FeMn ribonucleotide reductase

### 3.1. Presentation

Ribonucleotide reductases (RNR) are present in all cellular organisms where they realize the synthesis of the four deoxyribonucleoside triphosphates (dNTPs) by substitution of the 2′-OH of a ribonucleoside di- or triphosphate by a hydrogen atom. The activation of the ribonucleotide is achieved in all RNRs by abstraction of the 3′-hydrogen of the ribose by a transient thiyl radical of the enzyme [31]. RNRs have been separated in three different classes according to the way they interact with dioxygen and generate the thiyl radical [32]. Class I RNRs, that are of interest in the present context, contain two non-identical dimeric subunits, R1 and R2, arranged as a $R1_2R2_2$ heterotetramer. The active thiyl radical is formed on an active cysteine in R1 through an electron transfer over 35 Å to a tyrosyl radical located in R2 [31]. Most of class I RNRs rely on a diiron site that uses dioxygen to generate the tyrosyl radical in R2. Indeed, reaction of dioxygen with the reduced diiron center leads eventually to the formation of a $Fe^{III}Fe^{IV}$ so-called "**X**" species that is responsible for oxidation of the neighboring tyrosine [33,34].

$$Fe^{II}Fe^{II}\cdots Tyr + O_2 + e^- \rightarrow Fe^{III}Fe^{IV}\cdots Tyr$$

$$Fe^{III}Fe^{IV}\cdots Tyr \rightarrow Fe^{III}Fe^{III}\cdots Tyr^{\bullet}\,(\mathbf{X})$$

Fig. 2 (top) illustrates the X-ray structure of the active site of *Escherichia coli* RNR in its oxidized form [35,36]. The two ferric ions are doubly bridged by an oxide and a glutamate (Glu115). $Fe_2$ is terminally bound by a histidine (His241), two glutamates (Glu204, Glu238) and a water molecule making it hexacoordinated. By contrast, $Fe_1$ is only pentacoordinated being terminally bound by histidine 118 and aspartate 84 in addition to a water molecule. One hydrogen of this water molecule interacts with the hydroxyl group of the active tyrosine Tyr122. This active site is embedded in a four-helix bundle to which all iron ligands are bound. This overall arrangement of the iron ligands is a common feature of most

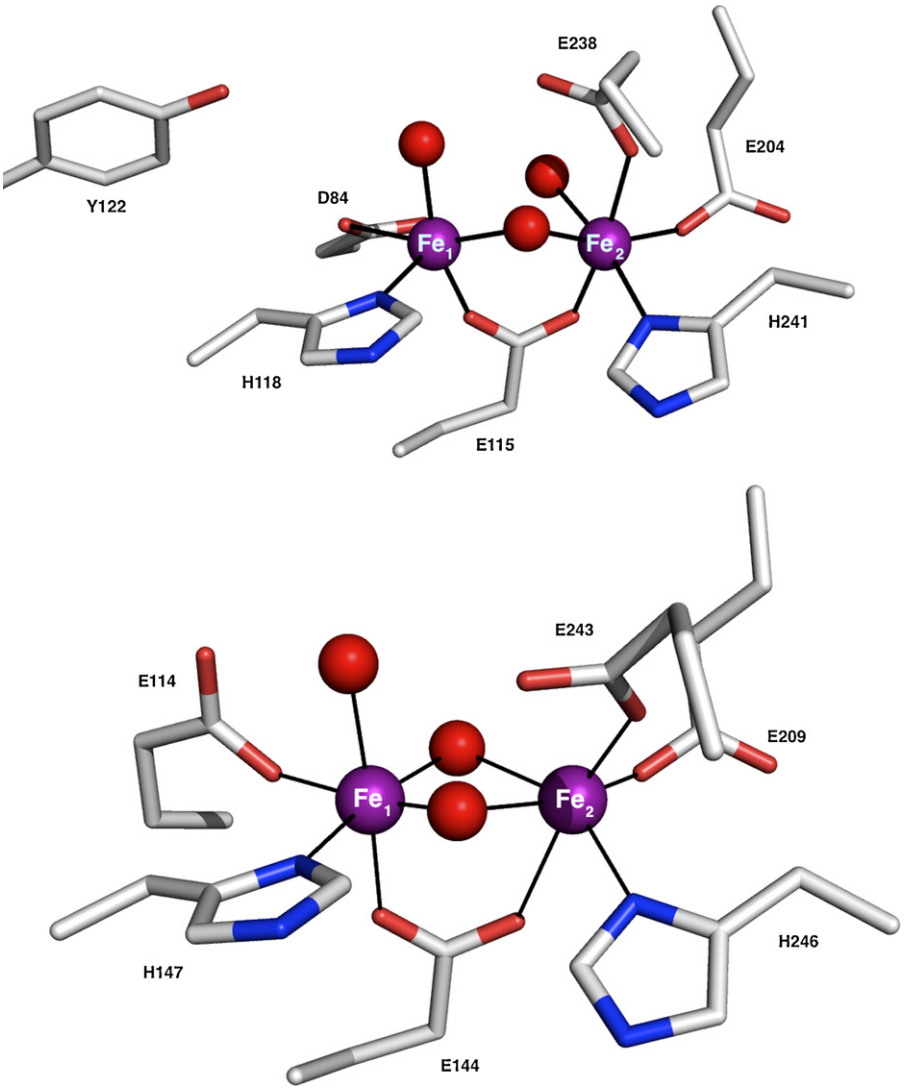


**Fig. 2.** Structure of the oxidized active sites of *Ec* RNR-R2 (top, PDB code: 1RIB) and *Mc* MMOH (bottom, PDB code: 1MTY) from [35,37], respectively. The iron atoms are colored in purple.

dioxygen activating enzymes with a dinuclear active site (Table 3) as shown for example for methane monooxygenase hydroxylase (MMOH) [37].

The X-ray structure of the active site of *Methylococcus capsulatus* MMOH in its oxidized form [37,38] is illustrated in Fig. 2 (bottom). It bears a strong resemblance with that of RNR-R2 but significant differences exist also. The two ferric ions are triply bridged by two hydroxides and a glutamate (Glu144) and they are both hexacoordinated. $Fe_2$ is terminally bound by the same three protein residues as in RNR-R2: a histidine (His246) and two glutamates (Glu209, Glu243). The coordination of $Fe_1$ differs from that observed in RNR-R2 and comprises a water molecule, a histidine (His147) and a glutamate (Glu114). It is worth noting that the water ligand is H-bonded to Glu114. By contrast, in RNR-R2 Glu114 is replaced by Asp84 and the water ligand is H-bonded to the active tyrosine Tyr122. The replacement of this glutamate by an aspartate is a distinctive feature of class I RNRs that is functionally significant.

**Table 3**
Metal ligands in the active sites of oxidized *M. capsulatus* MMOH, *E. coli* RNR-R2, *C. trachomatis* RNR-R2, *S. thioluteus* AurF and *M. tuberculosis* oxidase. Wat stands for a water molecule.

| Protein | Terminal ligands to $Fe_2$ | Bridging ligands | Terminal ligands to $M_1$[a] |
|---|---|---|---|
| *Mc* MMO | H246, E209, E243 | $(\mu\text{-OH})_2$, E144 | H147, E114 |
| *Ec* RNR | H241, E204, E238, Wat | $(\mu\text{-O})$, E115 | H118, D84, Wat |
| *Ct* RNR | H230, E193, E227 | $(\mu\text{-OH})_2$, E120 | H123, E89, Wat |
| *St* AurF | H230, E196, E227 | $(\mu\text{-O})$, E136 | H139, H223, E101 |
| *Mt* Oxidase | H205, E167, E202 | $(\mu\text{-O})$, E101 | H104, E68 |

[a] M is Fe for all proteins except *Mt* oxidase.

Class I has been subdivided in two subgroups, Ia and Ib, the latter being identified by the presence in its genome of a redoxin and an additional protein of still unknown function [32].

While a diiron center has been definitely associated with class Ia RNRs, the nature of the metal cofactor of class Ib enzymes has been a matter of controversy [39] and is still debated. Indeed, it was reported that class Ib RNRs from *Corynebacteriae* possessed a dimanganese cofactor [39] but this statement was contradicted [40]. Nevertheless, experimental evidence for the occurrence of such a cofactor in a class Ib enzyme from *E. coli* was very recently advanced [41].

A new subclass Ic within class I RNRs was discovered recently [42] and eventually shown to operate on a mechanism different from classes Ia and Ib, that involves an FeMn cofactor [12]. The emergence of subclass Ic RNRs originated when sequence alignments showed that in the RNR from the obligate pathogen

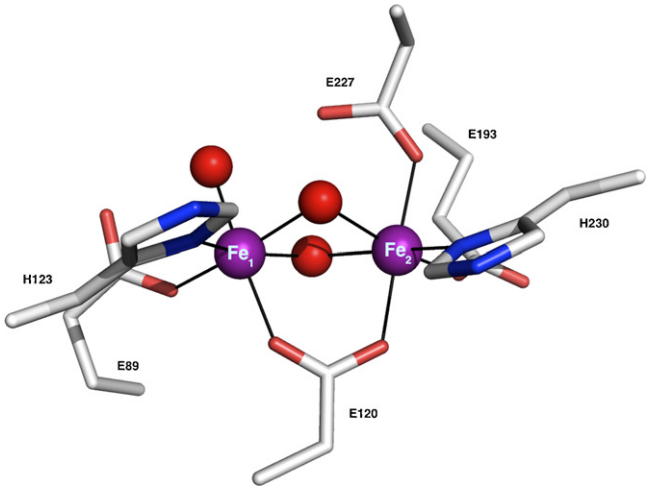


**Fig. 3.** X-ray structure of the oxidized active site of *Ct* RNR-R2 (PDB code: 1SYY) from [42]. The iron atoms are colored in purple.

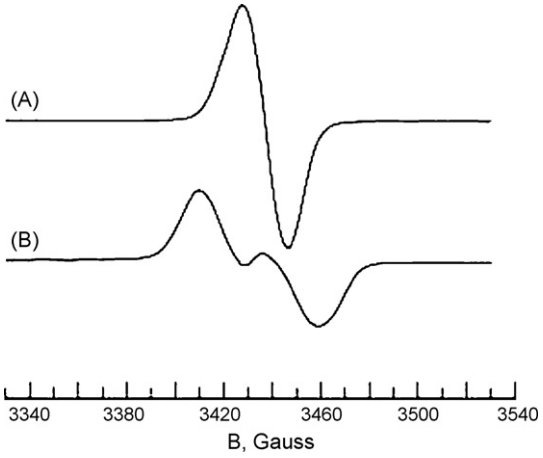


**Fig. 4.** EPR spectra of *Ct* RNR-R2 reconstituted with $^{56}$Fe (A) and $^{57}$Fe (B). Reproduced with permission from [42].

*Chlamydia trachomatis* a phenylalanine was found in place of the active tyrosine [43]. This observation was surprising in view of the fact that mutation of the active tyrosine by a phenylalanine in mouse RNR-R2 abolished the activity [44]. This mutation is present in diverse organisms including various pathogens and extremophiles [42].

### 3.2. Structural and physical characterization

#### 3.2.1. Experimental evidence supporting a diiron enzyme

The R2 subunit from *C. trachomatis* was expressed in *E. coli* [43] and crystallized. Its X-ray structure revealed an important overall similarity with class I RNR-R2 proteins, but even more, in some respects, with *M. capsulatus* MMOH (Table 3) [42]. All the active site residues are located in a four-helix bundle in the core of the protein. The two Fe atoms are bridged by two hydroxides and a glutamate (Glu120). Both Fe ions are hexacoordinated. $Fe_2$ is bound by a histidine (His230) and two glutamates (Glu193, Glu227) while $Fe_1$ is bound by a water molecule in addition to a histidine (His123) and a glutamate (Glu89). As mentioned above, residue Asp84 in *E. coli* RNR-R2 is H-bonded to the active tyrosine Tyr122 and is crucial for the protein activity (Fig. 3).

It is significant that in *C. trachomatis* that lacks the active tyrosine (replaced by phenyalanine Phe127), the aspartate is replaced by a glutamate (Glu89) that is engaged in quite different H bonds. A further difference with *E. coli* RNR-R2 resides in the bridging pattern of the two Fe ions. Indeed, it matches that of *M. capsulatus* MMOH with two hydroxides and a glutamate instead of the classical (μ-oxo)(μ-glutamato) pattern associated with class Ia RNR-R2 subunits.

The requirement for Fe was deduced from the observation that the protein expressed in presence of EDTA contained 0.75 Fe per polypeptide. Moreover, when the apoprotein was reacted with three equivalents $Fe^{2+}$ under aerobic conditions, a singlet EPR signal was detected (Fig. 4A) whose properties ($g$ = 1.999, line width ca. 18 G) matched those of *E. coli* intermediate **X** [34]. In particular, when $^{57}$Fe was used in the reconstitution procedure, the EPR spectrum exhibited the 26 G hyperfine splitting (Fig. 4B) characteristic of intermediate **X**. The intensity of this signal was clearly dependent on the Fe content but never exceeded 1/3 of the polypeptide concentration.

The origin of this signal was thoroughly investigated through a combination of EPR and $^{57}$Fe-, $^{14}$N- and $^{1}$H-ENDOR studies [45]. All these data point to a strong similarity with the corresponding parameters and therefore electronic structure of intermediate **X** from *E. coli* RNR-R2 [34]. However, very different stabilities were noted. While intermediate **X** of mouse RNR-R2 decays within 200 ms through electron abstraction from the active tyrosine [46], *C. trachomatis* intermediate **X** may be stabilized for several seconds and even minutes in certain conditions where excess R1 subunit and substrate are present [45,47]. An increased stability of intermediate **X** had been noted for mutants where the active tyrosine was replaced by a phenylalanine [34,44]. The decay of this signal does not generate an EPR active species. Moreover, this signal was observed on samples frozen during catalysis. These data led Gräslund et al. to suggest that an $Fe^{III}Fe^{IV}$ intermediate **X** may be the species responsible for generating the thiyl radical [48].

#### 3.2.2. Experimental evidence supporting an iron–manganese enzyme

The modest overall activity and the limited production of intermediate **X** (≤30% of the total protein) led Bollinger, Krebs et al. to reinvestigate the metal dependence of *C. trachomatis* RNR-R2 [12]. By combined reduction and EDTA chelation they were able to almost totally deplete *C. trachomatis* RNR-R2 from Fe ions and to reconstitute it. Interestingly, they found that the enzymatic activity does not correlate to the iron content, enzyme preparations with the same Fe content exhibiting activities differing by an order of magnitude. By contrast, they observed that the simultaneous addition of Fe and Mn to apo-RNR caused a 50-fold enhancement of the enzyme activity. Most importantly, they noted that the maximum activity is obtained for a 1:1 Fe:Mn ratio, as illustrated in Fig. 5A.

Moreover, when this ratio is maintained constant at Fe:Mn = 1, the enzyme activity is maximized at a metal:protein ratio of 2 (Fig. 5B). These observations clearly indicate the presence of a FeMn pair at *C. trachomatis* RNR-R2 active site, that will be further proven by spectroscopic studies.

The active form of the FeMn pair was generated by reacting the reduced pair $Fe^{II}Mn^{II}$ with $O_2$ and analyzed by EPR and Mössbauer spectroscopies. No EPR signal could be detected. As shown in Fig. 6A the 4 K Mössbauer spectrum of this species recorded in absence of applied magnetic field consists in a quadrupole doublet with parameters ($\delta$ = 0.52 mm/s, $\Delta E_Q$ = 1.32 mm/s) that are characteristic of a high-spin $Fe^{III}$ ion. The broadening of the signal recorded under a small magnetic field indicates that this ferric ion belongs to a paramagnetic species with an integer spin (Fig. 6B). The spin Hamiltonian parameters of this species are listed in Table 4. These spectroscopic data suggest that the active enzyme is a $Fe^{III}Mn^{IV}$ species.

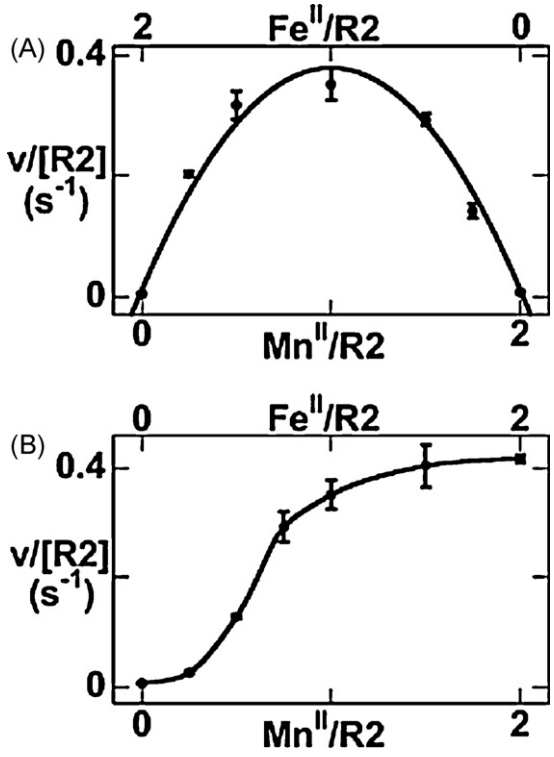


**Fig. 5.** Dependence of the catalytic activity of *Ct* RNR-R2 (A) on the Fe:Mn ratio at metal:protein ratio = 2 and (B) on the metal:protein ratio at constant Fe:Mn = 1. Reproduced with permission from [12].

**Table 4**
Spin Hamiltonian parameters of the various $Fe^xMn^y$ centers from *C. trachomatis* RNR-R2.

| | $Fe^{III}Mn^{III}$ | $Fe^{III}Mn^{IV}$ | $Fe^{IV}Mn^{IV}$ |
|---|---|---|---|
| $g$ | 2.030, 2.020, 2.015 | | 2.017, 2.030, 2.027 |
| $\mathbf{A}_{Fe}$ (MHz) | −64.5, −64.5, −64.5 | −55.4, −53.6, −53.2 | −55.9, −59.3, −40.5 |
| $\mathbf{A}_{Mn}$ (MHz) | 269, 392, 314 | | 247, 216, 243 |
| $\delta$ (mm/s) | 0.50 | 0.52 | 0.17 |
| $\Delta E_Q$ (mm/s) | 0.81 | 1.32 | −0.75 |
| $\eta$ | | | −10 |

Treatment of the active form of the FeMn pair with dithionite does not change the oxidation state of the Fe ion as deduced from its Mössbauer parameters ($\delta = 0.50$ mm/s, $\Delta E_Q = 0.81$ mm/s; Fig. 6C). By contrast, the species becomes EPR active in agreement with an $S = 1/2$ state exhibiting $^{55}$Mn hyperfine coupling (Fig. 7A and D). Simulation of these spectra revealed an anisotropic $\mathbf{A}_{Mn}$ tensor consistent with a $Mn^{III}$ ion. Spectra B, E and G of Fig. 7 have been recorded with $^{57}$Fe enriched samples and exhibit the expected additional coupling resulting from the interaction of the electronic spin with an $I = 1/2$ nucleus. Simulation of spectrum E revealed an isotropic $\mathbf{A}_{Fe}$ tensor in agreement with a high-spin $Fe^{III}$ ion. The spin Hamiltonian parameters of this species are listed in Table 4. This spectroscopic analysis establishes that dithionite treatment of the active enzyme produces a $Fe^{III}Mn^{III}$ species, in agreement with the hypothesis that the active form involves an $Fe^{III}Mn^{IV}$ center.

This conclusion was reached independently by Gräslund et al. [49]. Indeed, these authors confirmed the higher activity of the FeMn form of the enzyme (over the $Fe_2$ form) observed by Bollinger et al. [12]. Interestingly, they observed a linear dependence of the activity on both the Fe and the Mn concentration.

Treatment of the active form of the FeMn pair with the substrate analog $N_3$-ADP, 2′-azido 2′-deoxy-adenosine 5′-diphosphate ($N_3$-ADP), generates spectra F and G of Fig. 7 that in addition to the

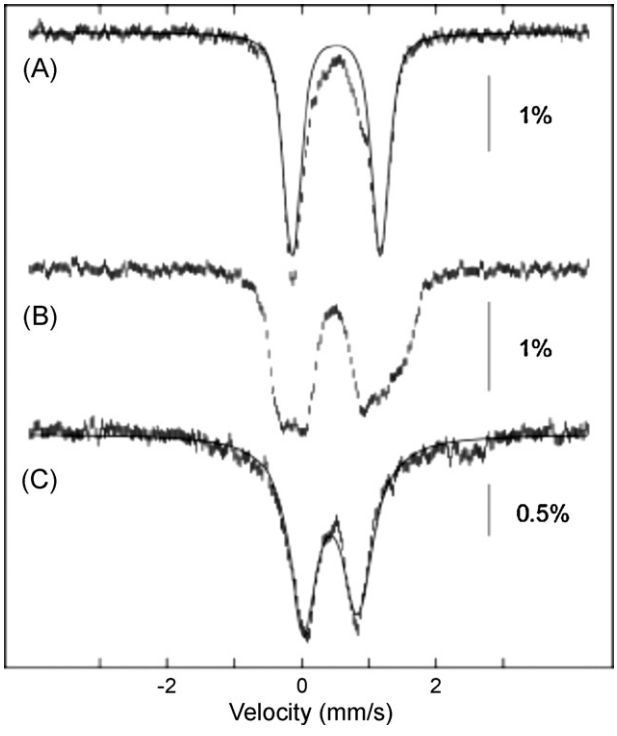


**Fig. 6.** Mössbauer spectra of the active form of *Ct* RNR-R2 at 4 K without applied magnetic field (A) and under a field of 53 mT applied parallel to the γ beam (B) and (C) at 190 K after dithionite reduction.
Reproduced with permission from [12].

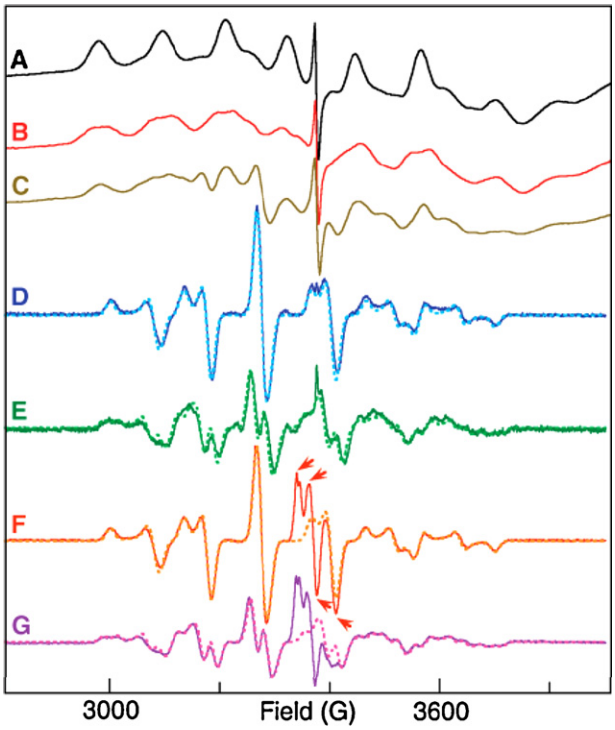


**Fig. 7.** EPR spectra of the active form of *Ct* RNR-R2 after dithionite reduction in the absence (A, B) or presence (C–E) of R1, cytidine 5′-diphosphate (CDP) and ATP or reaction with $N_3$-ADP (F, G), at 4 K (A–C) or 14 K (D–G) (see text for conditions).
Reproduced with permission from [12].

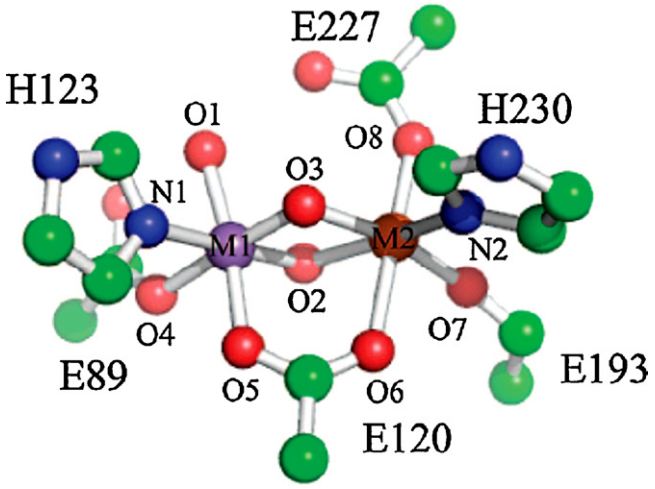


**Fig. 8.** DFT optimized model of the $Fe^{IV}Mn^{III}$ active form of *Ct* RNR-R2. Reproduced with permission from [51].

features of D and E exhibit resonances attributed to the nitrogen radical formed from $N_3$-ADP (see arrows in Fig. 7F and G). These experiments establish unequivocally that the $Fe^{III}Mn^{IV}$ state of the pair is the active form of *C. trachomatis* RNR-R2.

This active form was further analyzed by Mössbauer and X-ray absorption spectroscopies (XAS). A thorough Mössbauer study using strong applied magnetic fields showed that the spin state of the FeMn pair is $S = 1$, in agreement with an antiferromagnetic coupling of the high-spin $Fe^{III}$ ($S = 5/2$) and $Mn^{IV}$ ($S = 3/2$) ions [50]. A nearly isotropic $\mathbf{A}_{Fe}$ tensor was determined as expected. The spin Hamiltonian parameters of this species are listed in Table 4. XAS studies were performed both at the Fe and Mn K-edges [51]. Key structural parameters deduced from this work include (i) a short Fe–Mn distance 2.92 Å, (ii) an Fe environment with four O/N donors at 1.96 Å and two at 2.11 Å and (iii) a Mn environment with a single O scatterer at 1.74 Å and four O/N donors at 1.95 Å.

These structural data and the Mössbauer parameters were used to validate and discriminate DFT models built from the X-ray structure of the $Fe^{III}Fe^{III}$ species [42]. The resulting model, illustrated in Fig. 8, involves a (μ-oxo)(μ-hydroxo)(μ-1,3-carboxylato) core where the bridging carboxylate is provided by E120. The combination of oxo and hydroxo bridges is the only one that fits the experimental FeMn distance, a result supported by the experimentally determined structures of the corresponding diiron complexes [52,53]. A terminally bound water molecule complements the coordination of site M1. However, the calculations could not assign the metal occupancy (Fe vs Mn) of each site [51].

### 3.2.3. Characterization of the activation and maintenance mechanisms of Ct RNR

Scheme 1 (top) illustrates the mechanism of activation of *E. coli* RNR that is believed to involve the formation of a peroxodiferric intermediate from reaction of dioxygen with the reduced $Fe^{II}Fe^{II}$ form of RNR-R2 [54]. One-electron addition to this species produces intermediate **X**, the nature of which is still under intense scrutiny using sophisticated spectroscopic methods [55]. The loss of the active tyrosyl radical leads to an inactive oxidized enzyme that can be reactivated by reduction to the reduced state and further reaction with $O_2$. It was recently shown that this maintenance process was important for the regulation of RNR activity [56]. These aspects are out of the scope of the present review.

The occurrence of corresponding redox forms of the FeMn centers of *C. trachomatis* RNR was investigated by Gräslund et al. using XAS spectroscopy [59]. Two enzyme forms were specifically studied: an oxidized form comprising a mixture of $Fe^{III}Mn^{III}$ (major form), and $Fe^{II}Mn^{II}$, $Fe^{II}Mn^{III}$, and $Fe^{III}Mn^{IV}$ centers, and a reduced form constituted by a mixture of $Fe^{II}Mn^{II}$ (major form), $Fe^{II}Mn^{III}$ and $Fe^{III}Mn^{III}$ centers.

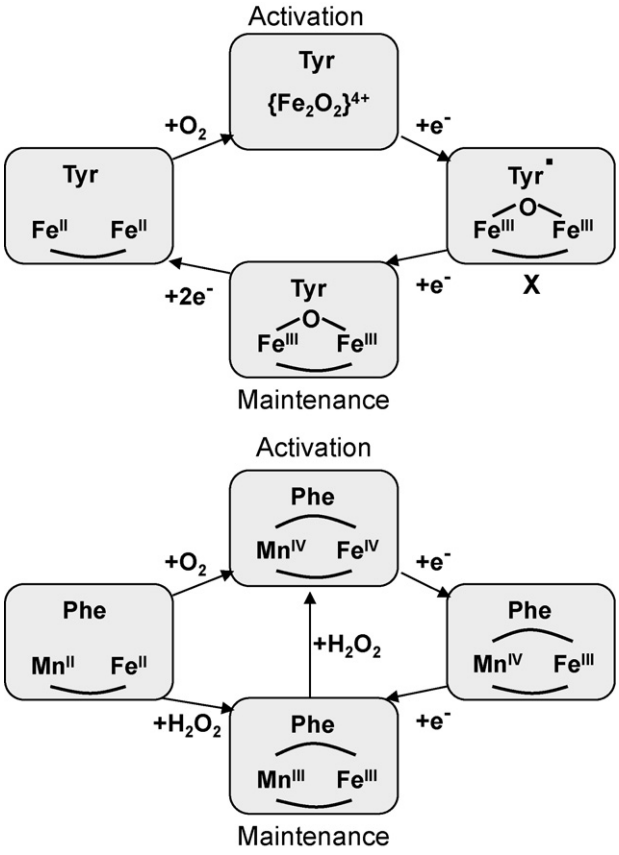


**Scheme 1.** Activation and maintenance mechanisms of *Ec* (top) and *Ct* (bottom) RNR adapted with permission from [57,58].

All these redox forms were quantified by combining EPR and XANES analyses. Tentative structures could be derived from EXAFS data. A feature of specific interest is the derived Fe–Mn distance that is characteristic of the bridging pattern. As expected this distance shortens as the oxidation states of the ions increase. For the $Fe^{III}Mn^{IV}$ active state the obtained 2.75 Å distance is significantly shorter than that determined by Green et al. (2.9 Å) [51]. It was proposed to be consistent with a (μ-oxo)(μ-hydroxo)(μ-1,3-carboxylato) core from the similar distance deduced from DFT calculations of *E. coli* RNR-R2 intermediate **X** [60]. Indeed these calculations estimate to 2.63 and 2. 82 Å the Fe–Fe distances in di(μ-oxo)(μ-1,3-carboxylato) and (μ-oxo)(μ-hydroxo)(μ-1,3-carboxylato) cores, respectively [60]. X-ray structure determinations of model complexes established for these cores significantly longer Fe–Fe distances: 2.71 and 2.84–2.89 Å for the di(μ-oxo)(μ-1,3-carboxylato) and (μ-oxo)(μ-hydroxo)(μ-1,3-carboxylato) cores, respectively [52]. Consequently, the structural meaning of the distance evaluated by Gräslund et al. [59] is ambiguous. Moreover, this distance was obtained from a sample where the $Fe^{III}Mn^{IV}$ center weighed only ca. 25%. Accordingly, the significance of these results may be questioned.

The lengthening of this distance (2.86–2.89 Å) in the $Fe^{III}Mn^{III}$ center is proposed to be due to the introduction of a two-atom bridging peroxide in a (μ-oxo)(μ-peroxo)(μ-1,3-carboxylato) core. Whereas introduction of such a peroxide into the core is likely to produce the observed effect no experimental evidence supporting it

has been provided [59]. It must be noted also that no accumulation of a peroxide intermediate has been detected during reaction of the active form either with dioxygen [61] or with hydrogen peroxide [62]. Consequently, the occurrence of a peroxo intermediate must not be considered as granted.

The increased 3.25 Å distance assigned to the $Fe^{II}Mn^{III}$ center is attributed to the loss of a bridging ligand resulting in a (μ-oxo)(μ-1,3-carboxylato) core. Finally the long distance (4.25 Å) observed in the reduced $Fe^{II}Mn^{II}$ center is consistent with the presence of a single carboxylate bridge. This hypothesis is supported by the observation that the EPR spectrum associated with this form consists of a six-line typical $Mn^{II}$ spectrum pointing to a very weak if any coupling with the neighboring $Fe^{II}$ ion [59].

The EPR properties of the *E. coli* RNR-R2 reconstituted with a $Fe^{II}Mn^{II}$ pair have been thoroughly studied. Owing to the different metal affinities of its two metal sites, *E. coli* RNR-R2 could be reconstituted by an heterometal pair and studied by MCD [63] and EPR [64,65] spectroscopies. Interestingly, it was shown that a $Mn^{II}$ ion could be introduced only in the site equivalent to site 2 of Fig. 8. The EPR signal of the resulting species strongly differs from that mentioned above [59] and shows the occurrence of a weak magnetic interaction ($-2J = 1.8\ cm^{-1}$) with the neighboring $Fe^{II}$ ion [65]. A different location of the Mn ion possibly related to the Glu vs Asp coordination at metal site 1 might be responsible for this difference.

The reaction of the reduced $Fe^{II}Mn^{II}$ form of *C. trachomatis* RNR-R2 with $O_2$ was investigated by stopped-flow and freeze-quench techniques to trap a high-valent intermediate precursor of the active $Fe^{III}Mn^{IV}$ enzyme. The reaction produces an EPR active species (Fig. 9) exhibiting a signal at $g \sim 2$ with a six-line splitting ca. 80 G indicative of hyperfine coupling to a $^{55}Mn$ nucleus [61]. This sextet is further split in samples prepared from $^{57}Fe$ owing to the hyperfine interaction with the $I = 1/2$ nucleus. Simulation of the EPR spectrum indicated a nearly isotropic $\mathbf{A}_{Mn}$ tensor in agreement with the $Mn^{IV}$ oxidation state. An extensive field-dependent Mössbauer study revealed parameters ($\delta = 0.17$ mm/s, $\Delta E_Q = -0.75$ mm/s) supporting an $Fe^{IV}$ formulation. This assignment was strengthened by the determination of a spin value of $S = 2$ and the evaluation of the intrinsic hyperfine tensor $\mathbf{a}_{Fe}$ whose values match those of the high-spin $Fe^{IV}$ of intermediate **X** from *E. coli* RNR-R2 [34].

The rates of formation and decay of this intermediate were monitored in UV–visible stopped-flow experiments through an intense absorption at 390 nm. The evolution of this band matched perfectly the evolution of the EPR signal. Formation of the intermediate is first-order in $[O_2]$ and the second order rate constant amounts to 13 (±3) mM $s^{-1}$. The addition of ascorbate does not influence the formation of the intermediate but accelerates its decay into the active form in a concentration-dependent manner.

The reaction of the reduced $Fe^{II}Mn^{II}$ form was investigated also with hydrogen peroxide and shown to proceed in three sequential steps: fast oxidation to $Fe^{III}Mn^{III}$, slower oxidation to $Fe^{IV}Mn^{IV}$ and decay to $Fe^{III}Mn^{IV}$. It was further shown that the $Fe^{III}Mn^{III}$ form itself can be reactivated by $H_2O_2$ and that the active form $Fe^{III}Mn^{IV}$ is stable to it [62]. All these transformations are included in Scheme 1 (bottom).

### 3.2.4. Summary and future work

The seminal work of Bollinger, Krebs et al. [57,58] has revealed the general mechanism of *C. trachomatis* RNR-R2 activity. The obvious question concerns the need for an FeMn center to replace the usual $Fe_2$ active site. The observation that these FeMn centers are present in pathogens led to the suggestion [42] that they may represent an adaptation to the defenses that the host mobilizes and in particular to nitric oxide. Indeed, NO is a well known inhibitor of RNRs through attack of the tyrosyl radical [66]. This view is supported by the observation that Mn import is a key part of *E. coli* response to oxidative stress that is related to Fe homoeostasis [67].

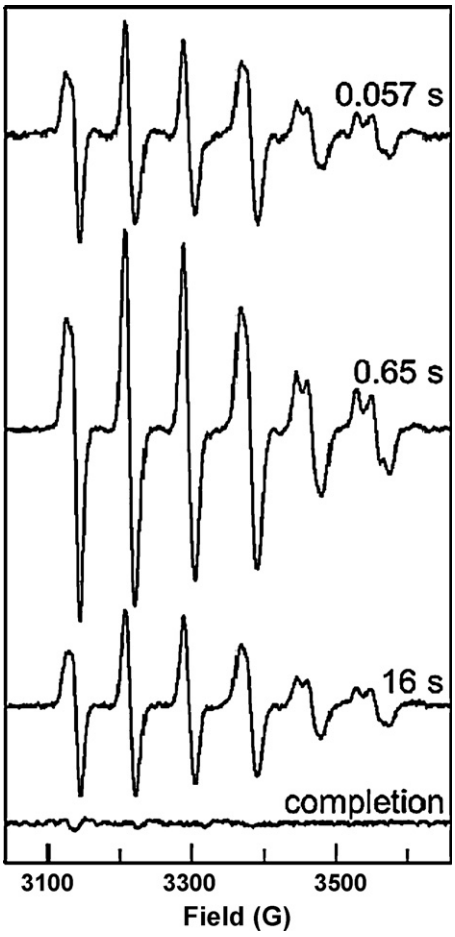


**Fig. 9.** X-band EPR spectra at 14 K of the of the $Fe^{IV}Mn^{IV}$ intermediate of *Ct* RNR-R2. Reproduced with permission from [61]. The delay before freezing of the sample is given on each spectrum.

In addition, with its lower oxidation potential [68] the FeMn center is intrinsically more stable. As far as further work is concerned, the absence of the active tyrosyl radical makes the radical transfer process to the active cysteine as well as activation, inhibition and maintenance processes easier to follow than in class Ia RNRs and opens the way to very detailed quantitative studies [58,69,70].

## 4. The arylamine oxygenase AurF

### 4.1. Presentation

This is a very recent and enlightening example of the difficulty in assessing the right metal atoms of an enzyme active site. Although, eventually, AurF is probably not an FeMn enzyme, it is included in this review because (i) it is both structurally and functionally related to RNR-R2 and MMOH and (ii) the lessons drawn from its studies have probably a farther reaching importance.

The *aurF* gene was discovered [71,72] as part of the *aur* operon of the fungi *Streptomyces thioluteus* HKI-227 that is involved in the biosynthesis of the rare nitroaryl polyketide metabolite aureothin (aur, Fig. 10).

It was shown to code for an N-oxygenase that is responsible for the transformation of the amino group of *p*-aminobenzoic acid (pABA) into the nitro substituent of *p*-nitrobenzoic acid (pNBA), a quite remarkable six electron oxidation. The reaction was proposed to occur as shown in Scheme 2 by sequential two-electron transfers leading successively to the hydroxylamine (pHABA) and the nitroso derivative [73].

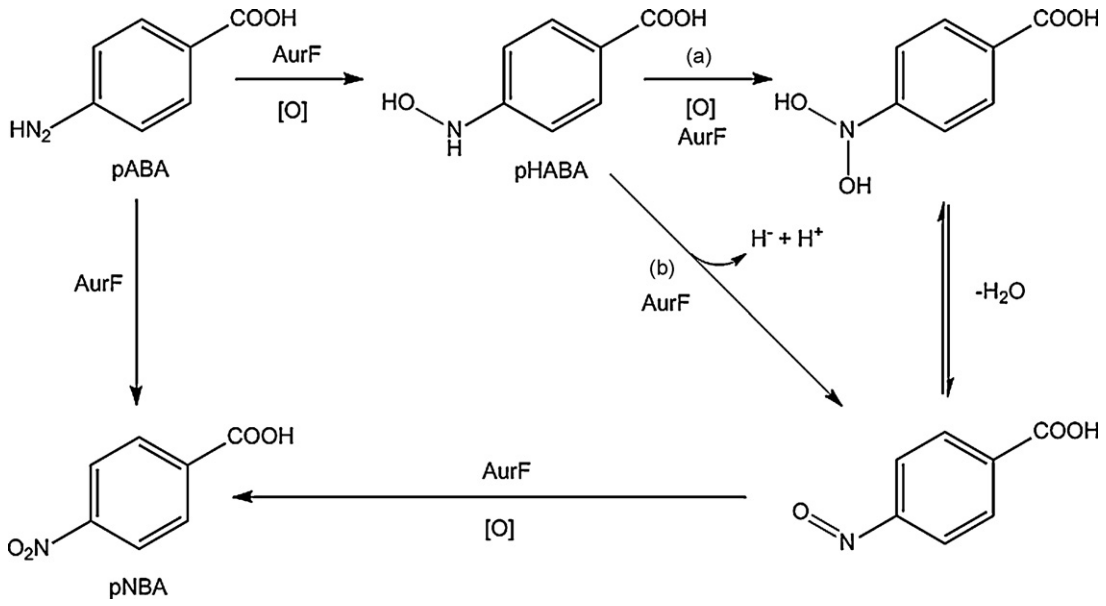


**Scheme 2.** Proposed biosynthetic pathway from pABA to pNBA via pHAB and *p*-nitrosobenzoic acid. Reproduced with permission from [74].

pHABA was detected in the reaction medium using a whole-cell assay and successfully used to produce pNBA, supporting that it is an actual intermediate. Interestingly, formation of the nitro product was five times faster starting from the hydroxylamine than from the amine itself. This observation led to propose that the first of the three oxidation steps (Scheme 2) is rate limiting. The nitroso derivative was not detected in these experiments [73].

Two different pathways can be envisaged for its formation (Scheme 2): either a dehydrogenation of the hydroxylamine, or its oxygenation into a dihydroxy species that is then dehydrated. The dehydrogenation pathway was shown to be operative through elegant $^{18}O$ labeling experiments [74]. Indeed, reacting the unlabeled hydroxylamine with $^{18}O_2$ would produce pNBA as a mixture of two $^{16}O^{18}O$ and $^{18}O^{18}O$ isotopomers if the reaction proceeded through a dehydration, whereas a single $^{16}O^{18}O$ monolabeled compound is expected for the dehydrogenation pathway. ESI-MS analysis of the reaction mixture pointed to the formation of only the monolabeled pNBA ruling out the dehydration pathway [74].

The nitroso derivative was eventually detected in separate in vitro experiments relying on the use of a reconstituted AurF enzyme expressed in *E. coli* [14].

### 4.2. Investigation of the nature of the metal site

#### 4.2.1. Early experimental evidence supporting a diiron enzyme

The nature of AurF active site was investigated initially through sequence alignments that revealed the conservation of several metal binding residues: histidines and aspartic and glutamic acids. Interestingly some of them were arranged as two copies of an $GluX_{28-37}Asp/GluX_2His$ motif that is well conserved in several diiron oxygenases, thus suggesting that AurF is a diiron enzyme [74]. This hypothesis was supported by two independent experiments. Zhao et al. overexpressed AurF in *E. coli* and prepared several site-directed mutants where each of the eight conserved residues were mutated to alanine. In agreement with this hypothesis, none of the mutants exhibited >1% activity of the wild type.

This hypothesis was further supported by iron titration that indicated 2.18 Fe atoms per protein and the observation of a rhombic EPR spectrum ($g_x$, $g_y$, $g_z$ = 1.94, 1.79, and 1.70) typical of $Fe^{II}Fe^{III}$ centers by dithionite reduction of the enzyme (Fig. 11B). The enzyme studied was a recombinant AurF isolated from *E. coli* and grown in Fe-supplemented minimal medium. Interestingly, the same enzyme grown in a Luria–Bertani medium exhibited a multiline EPR spectrum (Fig. 11A) similar to that observed for *E. coli* RNR-R2 containing a FeMn center [64].

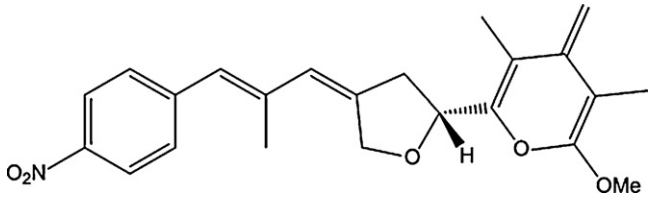


**Fig. 10.** Aureothin 1, antitumor and antifungal metabolite produced by *Streptomyces thioluteus*.

#### 4.2.2. Experimental evidence supporting a dimanganese enzyme

AurF was successfully expressed in *E. coli* as a fusion with a maltose-binding protein that was later cleaved. The enzyme was crystallized and the X-ray structure (Fig. 12) revealed that it is a $C_2$-symmetric homodimer containing 11 helices [75]. The active site is located within a set of four helices, which is characteristic of diiron proteins [8]. As in these proteins, each metal in AurF active site is bound by a carboxylate-imidazole pair belonging to the conserved sequence motif $(Asp/Glu)X_2His\text{-}X_n\text{-}(Asp/Glu)X_2His$ with n close to 100. In addition, a chain fold comparison identified *E. coli* RNR-R2 as its closest relative.

The active site consists in a dimanganese center where the Mn ions are distant from 3.6 Å and bridged by two glutamates (Glu136, Glu227) and an oxygen ligand ($H_2O$ or $OH^-$) [76]. The bridging modes of the two glutamates differ: Glu136 bridges the Mn ions in the μ-1,3 mode through its two O atoms while Glu227 both chelates $Mn_2$ and bridges $Mn_1$ and $Mn_2$ through the μ-1,1 mode. $Mn_1$ is terminally bound to two histidines (His139, His223) and a glutamate (Glu101) while $Mn_2$ is terminally bound to one histidine (His230) and a glutamate (Glu196). While each metal is bound by the consensus $GluX_2His$ motif $Mn_1$ is bound by an additional histidine (His223) that is strictly conserved in these enzymes. A BLAST sequence search identified a dozen bacterial sequence-related proteins that were still annotated "hypothetical". All of these proteins

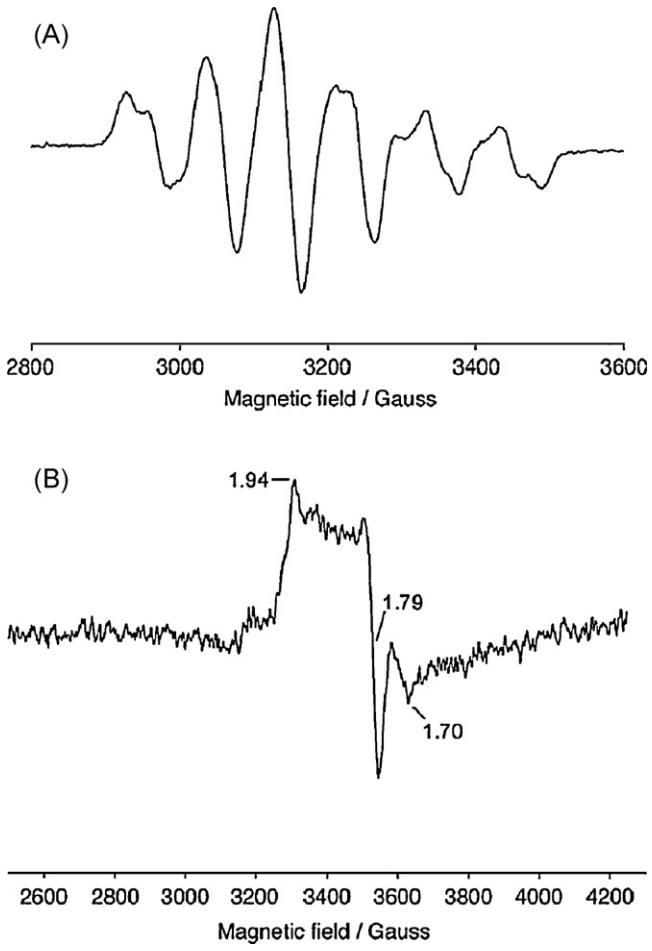


**Fig. 11.** EPR spectra of oxidized (A) and reduced (B) *St* AurF (see text for conditions). Reproduced with permission from [74].

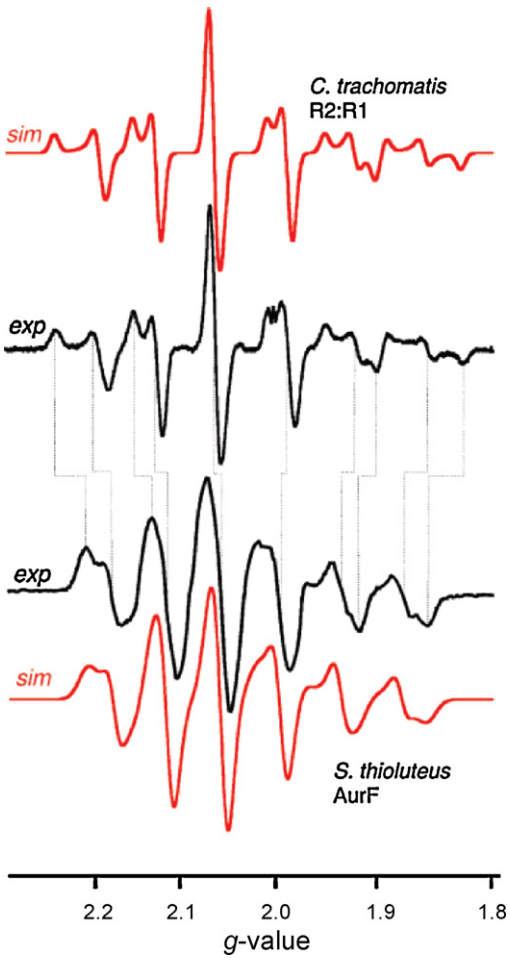


**Fig. 13.** Comparison of the EPR spectra of the $Mn^{III}/Fe^{III}$ of *Ct* RNR-R2 and the oxidized form of *St* AurF.
Reproduced with permission from [13].

possess the additional histidine ligand corresponding to His223 in AurF, that is not present in dioxygen activating diiron enzymes (Table 3).

The influence of the Fe:Mn ratio in the culture medium on the metal content and the enzymatic activity was studied systematically. Metal titration showed that an enzyme grown at a Fe:Mn ratio of 3:1 contained 15% of Fe. This translates into a 20-fold preference for Mn over Fe, which was attributed to the presence of the additional histidine in AurF active site [75]. On the other hand, variation of the Fe/Mn ratio over a 256 range did not result in significant change of the enzymatic activity. The enzyme exhibited the EPR signature of mononuclear $Mn^{2+}$ that can originate from a dinuclear center with a single carboxylate bridge [77]. This signal disappeared upon reaction with $H_2O_2$ to give a sharp radical signal, thus suggesting that the Mn center is active. Nevertheless, the possibility that the activity be associated with an Fe center was not ruled out since the enzyme sample still contained 15% iron [75].

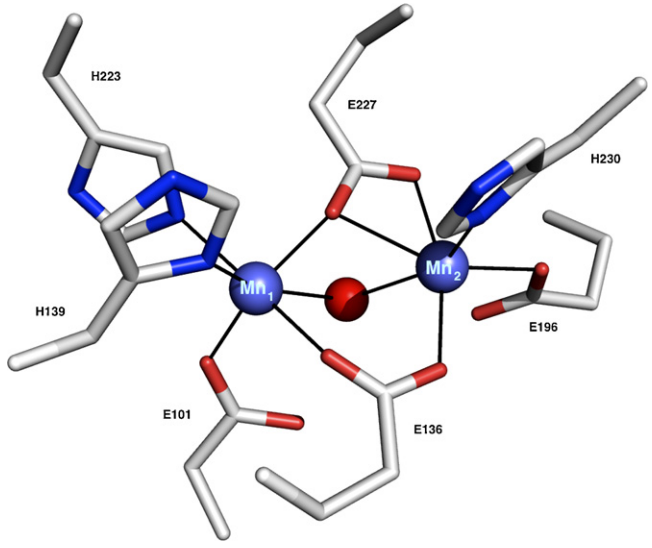


**Fig. 12.** X-ray structure of the dimanganese active site of *St* AurF (PDB code: 2JCD) from [76]. The manganese atoms are colored in blue.

### 4.2.3. Experimental evidence supporting an iron–manganese enzyme

Bollinger, Krebs et al. [13] analyzed in depth the Mn EPR spectrum (Fig. 12A) detected by Zhao et al. [74]. Simulation of the spectrum (Fig. 13) gave parameters ($\mathbf{A}_{Mn}$ (MHz) = (210, 270, 322 MHz) and $g$ = 2.030, 2.014, 2.015) consistent with the values expected for a $Mn^{III}$ ion antiferromagnetically coupled to a high-spin $Fe^{III}$ ion, resulting in a $S = 1/2$ ground state. The derived intrinsic hyperfine tensors ($\mathbf{a}_{Mn}$ (MHz) = (−158, −203, −242) of the $Mn^{III}$ ion are smaller than those of the $Fe^{III}Mn^{III}$ form of *C. trachomatis* RNR but very similar to those of the $Mn^{III}Mn^{IV}$ form of *Thermus thermophilus* catalase [78].

These authors performed an independent sequence search that expanded the group of similar proteins identified by Zhao et al. [74]

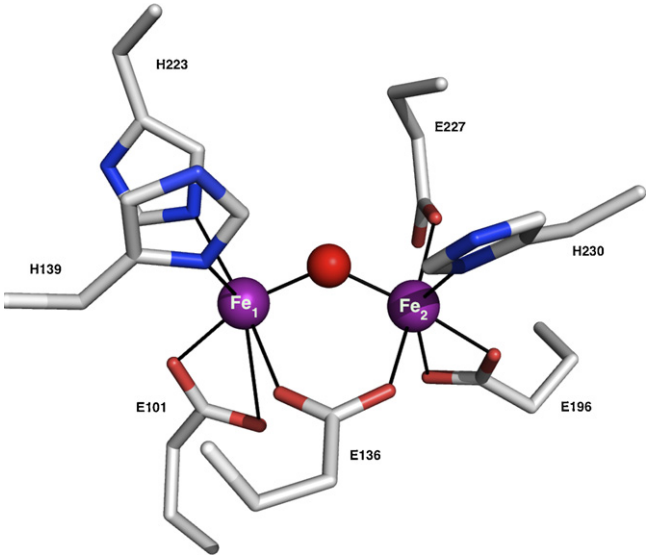


**Fig. 14.** X-ray structure of the diiron active site of *St* AurF (PDB code: 3CHI) from [14]. The iron atoms are colored in purple.

and Hertweck et al. [75]. From these EPR and sequence data they proposed that AurF is a FeMn enzyme and that the site bearing the additional histidine is that binding the Mn ion.

#### 4.2.4. Experimental evidence supporting a diiron enzyme

Zhao et al. reported a second crystallographic study of AurF (Fig. 14) that was performed on an oxidized diiron enzyme [14]. While most structural features are conserved with the preceding structure, a few differences exist that deserve to be emphasized. The two Fe ions are bridged by an oxo ligand (identified by short Fe–O bond distances) and a single μ-1,3 glutamate (E136). Indeed, the μ-1,1 glutamate bridge (E227) of the preceding structure has become terminally bound to $Fe_2$. The same kind of "carboxylate shift" [79] occurs in MMOH: Glu243 that acts as bridging ligand and terminal ligand on one Fe in reduced MMOH becomes terminal on this Fe ion in the oxidized form [8].

At $T = 4$ K the fully reduced AurF exhibits an EPR signal in parallel mode at $g = 16$ that is characteristic of a ferromagnetically coupled diferrous pair as found in reduced MMOH [80].

Being able to obtain the reduced form allowed the authors to study the enzymatic activity of reconstituted AurF. Of special interest is the study of AurF activity when grown in minimal medium with different Fe:Mn ratios. These experiments clearly showed that the maximum activity (0.13–0.16 units/mg AurF) is obtained in the absence of Mn. By contrast, the best activity reported for the dimanganese enzyme is only 0.0032 units/mg AurF [75], or ca. 2–2.5% of the diiron enzyme. This comparison leads credence to the fact that the reported activity of the dimanganese enzyme is due to the remnant Fe ions and that a diiron pair is AurF physiological cofactor.

### 4.3. Oxygen transfer mechanism

The pathway for the oxygenation of the amino group has been fairly well delineated with characterization of the two intermediates [73,74]. By contrast, the dioxygen activation process has just started to be investigated, following the sound assignment of the diiron cofactor. Bollinger, Krebs et al. [81] developed a combination of stopped-flow and Mössbauer freeze-quench experiments to trap and characterize an active intermediate in the reaction of reduced AurF and $O_2$. At first, these authors characterized the as-isolated diiron AurF overproduced in *E. coli* as a mixture of a μ-oxo

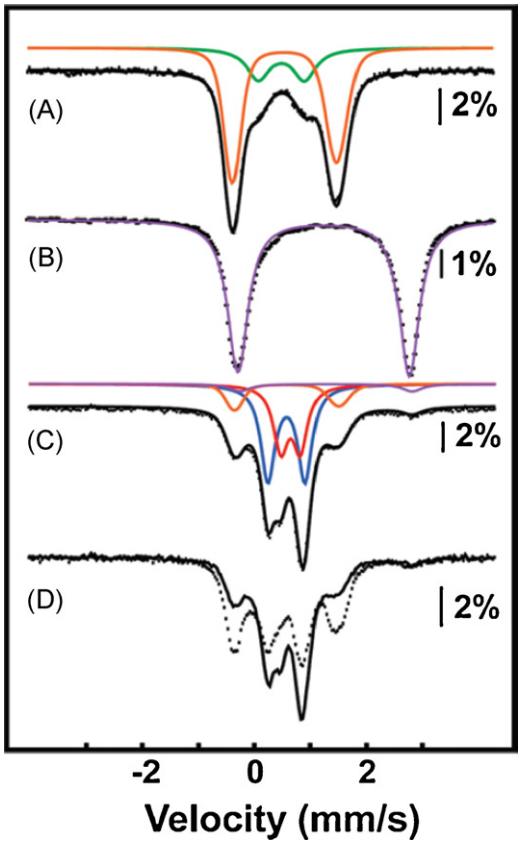


**Fig. 15.** Mössbauer spectra of as-isolated AurF (A); dithionite-reduced AurF (B); dithionite-reduced AurF exposed 2 min to $O_2$ and frozen (C) or reacted with 0.3 equiv. pABA before freezing (D). Solid lines are simulation. Color lines indicate the deconvolutions into the different components: μ-oxo (orange), μ-hydroxo (green), reduced (purple), peroxo (blue).
Reproduced with permission from [81].

and probably a μ-hydroxo diferric centers, identified from their Mössbauer parameters (μ-oxo: $\delta = 0.54$ mm/s, $\Delta E_Q = -1.86$ mm/s; μ-hydroxo: $\delta = 0.48$ mm/s, $\Delta E_Q = 0.80$ mm/s; Fig. 15A). Dithionite reduction gave the reduced enzyme with a symmetrical high-spin ferrous pair ($\delta = 1.24$ mm/s, $\Delta E_Q = 3.06$ mm/s; Fig. 15B). In this process the 350 nm absorption of the μ-oxodiferric species is bleached.

Exposure to dioxygen at 20 °C produces a new absorption at 500 nm that is fully developed in 0.01 s and does not decay appreciably over 100 s. Mössbauer analysis of this species shows that apart from the starting diferrous form (5%) and the μ-oxodiferric form (18%) the spectrum is constituted by a pair of doublets with parameters typical of high-spin ferric ions ($\delta = 0.54$ mm/s, $\Delta E_Q = -0.66$ mm/s; $\delta = 0.61$ mm/s, $\Delta E_Q = 0.35$ mm/s; Fig. 16C). Mössbauer experiments under high magnetic field reveal that these doublets are associated with a diamagnetic ground state, indicating that the ferric ions are antiferromagnetically coupled. They are assigned to isomeric peroxodiferric species. Reactivity studies showed that while this species is stable ca. 7 min in absence of substrate, it decays rapidly in presence of one equivalent pABA ($k_{obs} = 150 \pm 20\ s^{-1}$), producing pNBA. The spectroscopic properties of this active peroxo intermediate differ from those of the μ-1,2-peroxo and μ-($\eta_2$,$\eta_2$)-peroxo diferric species formed in RNR-R2 [82,83] or MMOH [83], respectively. By contrast, they appear similar to those of toluene/o-xylene monooxygenase for which the peroxo complex has been proposed to behave as an electrophile attacked by the aromatic substrate [84]. This led to the suggestion that AurF peroxo species could be attacked by the nucleophilic aniline nitrogen. This electrophilic character of the peroxo species

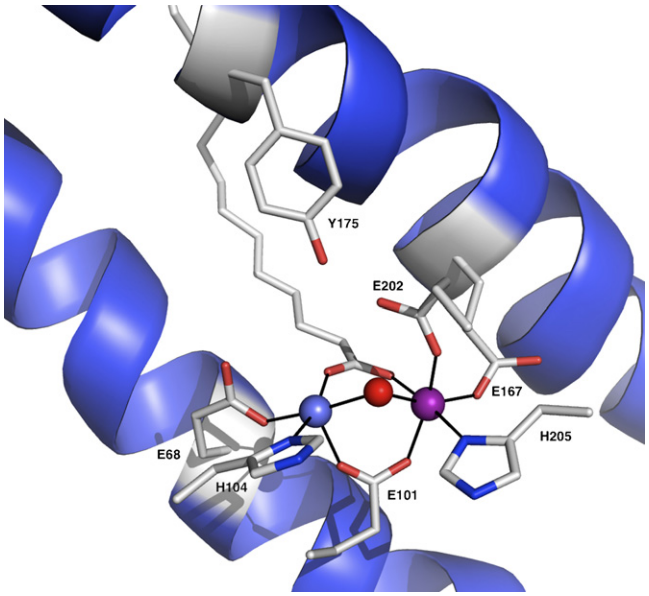


**Fig. 16.** X-ray structure of the active site of *Mt* oxidase (PDB code: 3EE4) from [85]. The iron and manganese atoms are colored in purple and blue, respectively.

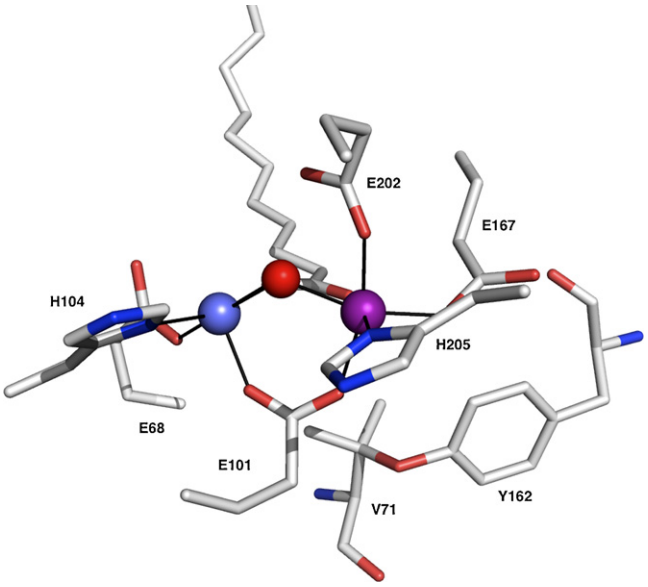


**Fig. 17.** X-ray structure of the active site of *Mt* oxidase showing the valine–tyrosine crosslink (PDB code: 3EE4) from [85]. The iron and manganese atoms are colored in purple and blue, respectively.

could be associated with a structure different from the above bridging ones and possibly involve a μ-1,1-hydroperoxo arrangement.

### 4.4. Conclusion

This survey has highlighted the difficulties encountered at times to identify the physiological metal of an enzyme. Eventually, it seems fairly well ascertained now that AurF possesses a diiron cofactor. This raises the question as to why manganese could be bound in place of iron [75]. The answer to this question may probably be found in the conditions of cell cultures, in particular the use of large metal concentrations [75]. One can hypothesize that such high concentrations are akin to a metal stress and are likely to disturb the metal homeostasis of the cell [3], eventually leading to a non-physiological behavior.

## 5. A new class of FeMn oxidases

Initial sequence alignments had identified a few proteins similar to *C. trachomatis* RNR and constituting the RNR Ic class [42]. This number has recently increased to ca. 50 allowing a more in-depth phylogenetic analysis (see below) that led eventually to the recognition of a new protein family. Andersson and Högbom very recently reported the X-ray structure [85] of a protein of this new family that they isolated from *Mycobacterium tuberculosis* and proposed to be an FeMn oxidase.

Importantly, when the Mn:Fe ratio in the expression media was changed from 1:10 to 100:1 the protein always contained close to one equivalent of each metal, establishing that it is a true FeMn protein. Its structure, depicted in Fig. 16, reveals several interesting and novel features. The Fe and Mn ions are unambiguously located: Mn is bound by two protein residues (Glu68, His104) whereas Fe is coordinated by three residues (Glu167, Glu202, His205). The two metal ions are triply bridged by a glutamate (Glu101), a water derived ligand, and the carboxylate group of myristic acid ($C_{13}H_{27}CO_2H$). This ligand is bound in a large cavity similar to that found in bacterial multicomponent monooxygenases [8].

Fig. 17 illustrates the second-sphere surrounding of the Fe ion, which shows a crosslink between Val71 and Tyr162 residues with the phenolic oxygen bound to the secondary carbon of the isopropyl group. Such a tyrosine–valine crosslink is unprecedented and witnesses the occurrence of an oxidation reaction. Indeed, this crosslink results from a two-electron oxidation removing two hydrogen atoms.

This protein bears a strong sequence and structure resemblance to class Ic *C. trachomatis* RNR-R2, however it failed to show any RNR activity. On the other hand, the observed Val71–Tyr162 crosslink indicates that it may perform oxidative transformations. In this respect, it is of interest to note the presence as a second-sphere residue of a tyrosine (Tyr175) that is H-bonded to Fe ligand Glu202 and situated at 4.9 Å from the Mn ion (Fig. 16). This tyrosine is close to the metal center and H-bonded to its ligand, as the active tyrosine in RNR-R2 s. However, whereas in class Ia RNR-R2 this tyrosine is protected from solvent in a hydrophobic pocket, in *M. tuberculosis* protein its oxygen lines the substrate-binding cavity, which opens the possibility that its oxidation may initiate the reactivity. Further work is needed to delineate the function of this novel class of proteins that make the link between ribonucleotide reductases [32] and bacterial multicomponent monoxygenases [8].

These structural results and a phylogenetic analysis of the 50 sequence-related proteins allowed Högbom [86] to discriminate two subfamilies from a few key sequence determinants. These two families were named R2c and R2lox from their respective parent proteins *C. trachomatis* RNR-R2 and *M. tuberculosis* oxidase. Their overall species distribution suggests that the FeMn cofactor is preferred by extremophiles and pathogens. This observation reinforces the hypothesis that the FeMn cofator is a natural response to stress conditions.

## 6. FeMn complexes

Heterodinuclear complexes have attracted interest either as potential models for PAP active sites or as a means to tuning the number of unpaired electrons involved in magnetic exchange interactions. A few FeMn compounds have thus been reported [87–94]. In this section, we will concentrate on those involving either phenoxo [88,90–92] or oxo [87,89] bridging ligands [95] (Scheme 3).

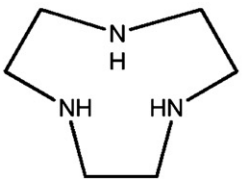

**L'**: 1,4,7-trimethyl-1,4,7,-triazacyclononane

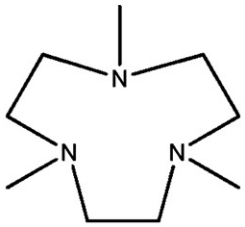

**L**: 1,4,7,-triazacyclononane

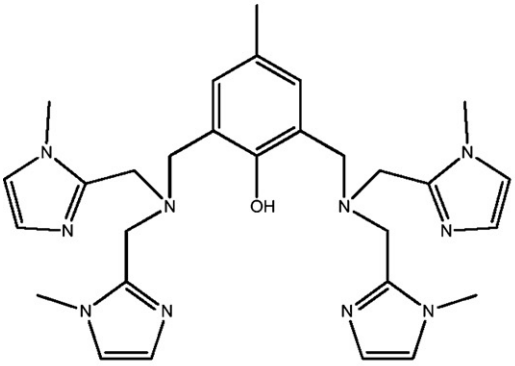

**H-BIMP**: 2,6-bis[(bis((1-methylimidazol-2-yl)methyl)amino)methyl]-4-methylphenol

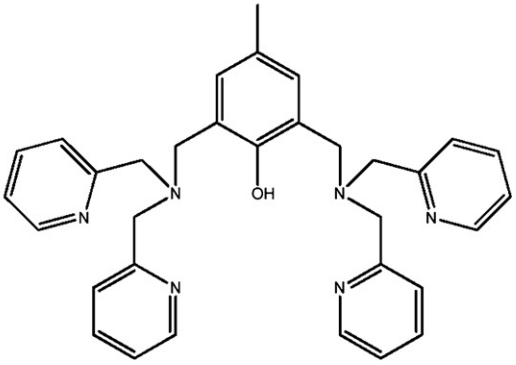

**H-BPMP**: 2,6-Bis[ (bis( 2-pyridylmethyl)amino)methyl]-4-methylphenol,

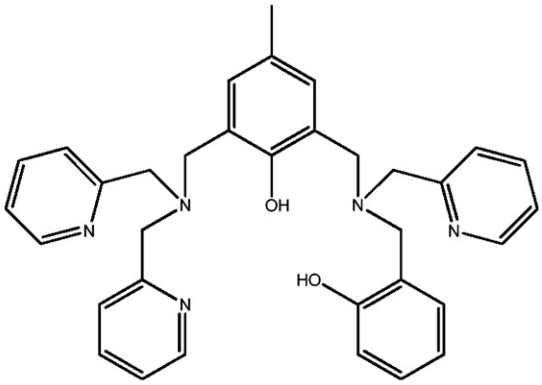

**$H_2$BPBPMP**: 2-bis[ {(2-pyridylmethyl)-aminomethyl}-6-{(2-hydroxybenzyl)-(2-pyridylmethyl)}-aminomethyl]-4-methylphenol

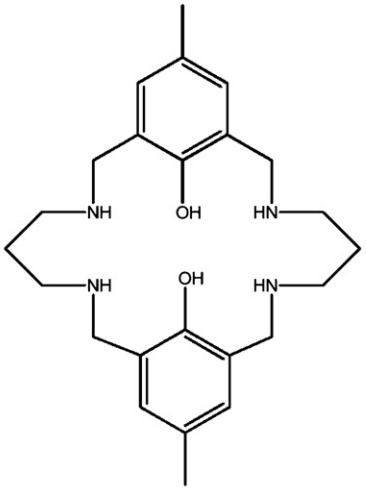

**μ-Mac:** tetramine-diphenol macrocyclic

**Scheme 3.** Structure of the ligands.

### 6.1. Oxo-bridged complexes

The first FeMn complex was reported by Wieghardt et al. [87] as part of their systematic investigation of oxo-bridged dinuclear complexes of first row transition metals aimed at rationalizing the observed magnetic exchange interactions [89].

The $Fe^{III}$ and $Mn^{III}$ ions were bridged by an oxide and two acetate ligands and capped by a 1,4,7-trimethyl-1,4,7,-triazacyclononane ligand (L′, Scheme 3) [87]. In addition unsymmetrical complexes were prepared with either the iron or the manganese ion bound by the unsubstituted 1,4,7,-triazacyclononane ligand (L, Scheme 3).

Fig. 18 illustrates the X-ray structure of the unsymmetrical complex with Fe bound by 1,4,7-trimethyl-1,4,7,-triazacyclononane. Short metal-oxo distances were noted as expected (Fe–O: 1.817 Å, Mn–O: 1.782 Å). The magnetic properties of the complexes were studied and indicated that the ferric ion is in the high-spin state.

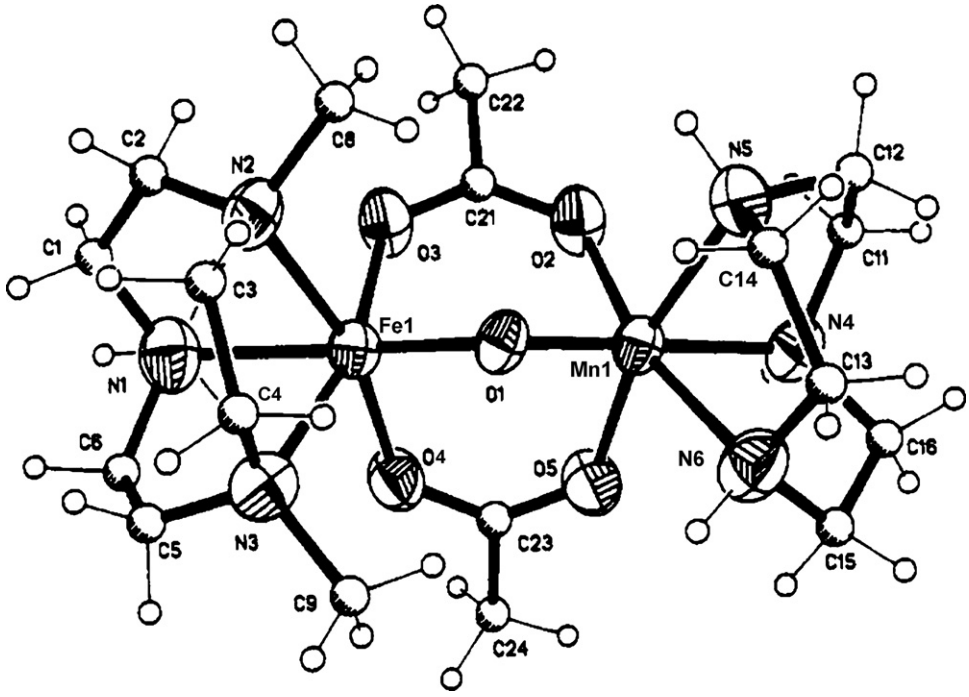


**Fig. 18.** X-ray structure of the complex cation $[L'Fe(\mu\text{-}O)(\mu\text{-}OAc)_2MnL]^{2+}$.
Reproduced with permission from [89].

Very strong antiferromagnetic exchange interactions were found ($-2J \sim 240$–$300\ cm^{-1}$) and attributed to strong overlap between the half-filled d orbitals on both Fe and Mn sites. A more elaborate theoretical treatment reproduced the strong antiferromagnetic interaction and attributed it to dominant "non-crossed" interactions $d_{xz}$–$d_{xz}$ and $d_{yz}$–$d_{yz}$ [96].

Oxidation of these compounds by peroxodisulfate was reported to give $Fe^{III}Mn^{IV}$ complexes. These compounds have not been fully characterized owing to the presence of substantial amounts of paramagnetic impurities. However, their reported UV–visible spectra resemble that of active *Ct* RNR-R2 thus leading credence to the assignment [61].

### 6.2. Phenoxo-bridged complex

A few μ-phenoxo FeMn complexes have been reported by groups interested in modelling proteins possessing a dimetal active site [88,90,92,97,98]. They were based on heptadentate ligands bearing multiamine donors on the ortho-phenolic positions as illustrated in Scheme 3. All these complexes possess a (μ-phenoxo)bis(μ-carboxylato) core. Que et al. were the first to report the synthesis of heterobimetallic complexes of this kind using the heptadentate ligand (H-bpmp) providing four terminal pyridines to the metal pair (Scheme 3) [90,97]. The $Fe^{III}Mn^{II}$ compound was not structurally characterized. The high-spin nature of the ferric ion was deduced from its Mössbauer parameters ($\delta = 0.45$ mm/s, $\Delta E = 0.49$ mm/s) [97]. A magnetic susceptibility study evaluated to $-2J = 23\ cm^{-1}$ the magnetic exchange interaction [90]. The complex can be reversibly reduced to the $Fe^{II}Mn^{II}$ state at the potential $E = 0.024$ V vs SCE ($E = -0.36$ V vs $Fc/Fc^+$).

In their modelling studies of PAP active site, Buchanan et al. reported the μ-phenoxo $Fe^{III}Mn^{II}$ complex of an analogous ligand (H-bimp) having 1-methyl-imidazole groups in place of the pyridines (Scheme 3) [88]. Fig. 19 illustrates the X-ray structure of the resulting complex. The charge balance and the structural data indicate that the FeMn pair is in the $Fe^{III}Mn^{II}$ valence state.

The physical properties of the complex were studied in the solid state and in solution. Mössbauer spectroscopy showed that the ferric ion is in the high-spin state ($\delta = 0.36$ mm/s, $\Delta E_Q = 0.65$ mm/s). Magnetic susceptibility measurements revealed a weak exchange interaction ($-2J = 16\ cm^{-1}$).

The electronic spectrum of the complex is dominated by an intense phenolate → $Fe^{III}$ charge transfer transition at 559 nm ($\varepsilon = 674\ M^{-1}\ cm^{-1}$). The complex could be reversibly oxidized to the $Fe^{III}Mn^{III}$ state at 0.69 V and reduced to the $Fe^{II}Mn^{II}$ state at −0.49 V (vs $Fc/Fc^+$). However, neither the oxidized nor the reduced species were characterized.

In order to mimic the binding of the terminal tyrosine of the PAPs, Neves et al. [92] resorted to the usual replacement of one pyridine of the H-bpmp ligand by a phenol group [99]. They thus obtained the unsymmetrical ligand H-bpbpmp (Scheme 3), com-

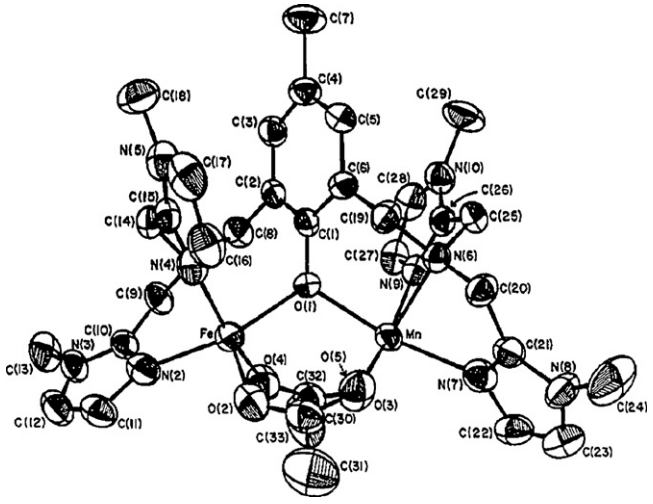


**Fig. 19.** X-ray structure of the complex cation $[FeMn(\mu\text{-}Bimp)(\mu\text{-}OAc)_2]^{2+}$.
Reproduced with permission from [88].

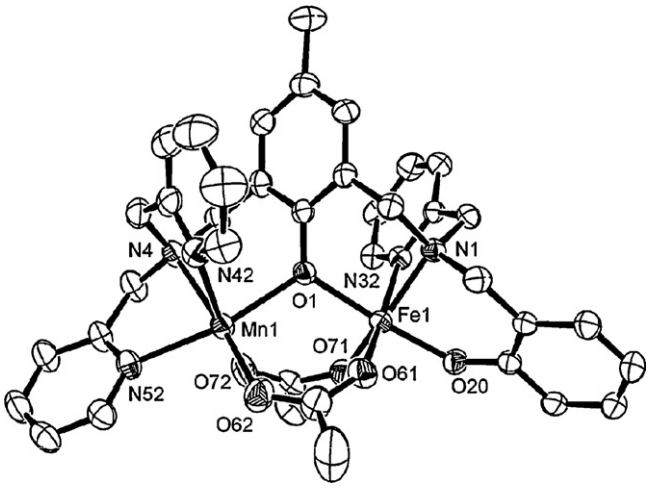


**Fig. 20.** X-ray structure of the complex cation [FeMn(μ-bpbpmp)(μ-OAc)$_2$]$^+$. Reproduced with permission from [92].

bining three pyridines and a phenol, and synthesized a $Fe^{III}Mn^{II}$ complex that reproduces the tyrosinate binding of the FeMn PAP. The X-ray structure of the complex is illustrated in Fig. 20.

The physical properties of this compound are very similar to those of Buchanan's complex [88]. Mössbauer spectroscopy indicates the high-spin nature of the ferric ion ($\delta = 0.48$ mm/s, $\Delta E_Q = 1.04$ mm/s). A weak antiferromagnetic exchange ($-2J = 14\ cm^{-1}$) is again evaluated by magnetic susceptibility.

Both a hypsochromic shift and a strong intensity increase are noted in the phenolate → $Fe^{III}$ charge transfer transition that is observed at 544 nm ($\varepsilon = 2680\ M^{-1}\ cm^{-1}$). This reflects the presence of the second phenoxo ligand. The complex could be reversibly oxidized to the $Fe^{III}Mn^{III}$ state at 0.44 V and reduced to the $Fe^{II}Mn^{II}$ state at −0.87 V (vs $Fc/Fc^+$). Neither the oxidized nor the reduced species were investigated. Interestingly, this compound proved active in the hydrolysis of the reference substrate 2,4-bis(dinitrophenyl)phosphate with a maximum efficiency at pH 6.7 and Michaelis–Menten kinetics. However, owing to the fact that both metal ions are hexacoordinated in the compound, it is likely that dissociation of some ligand (probably acetate) must occur for the catalysis to operate [92].

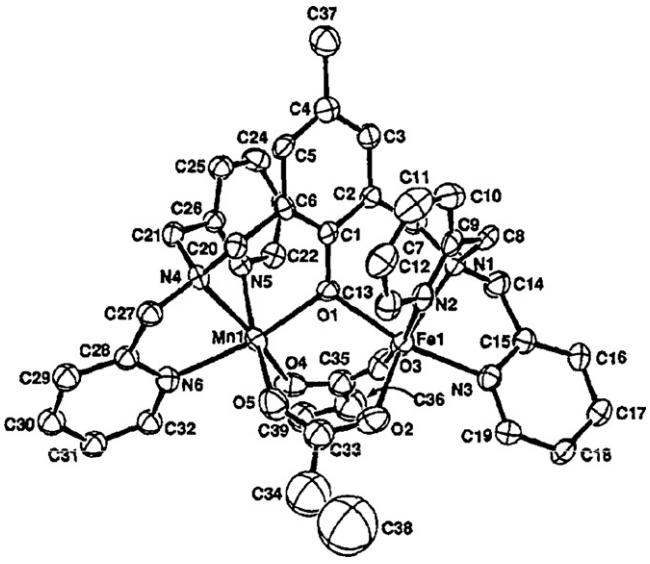


**Fig. 21.** X-ray structure of the complex cation [FeMn(μ-bpmp)(μ-OPr)$_2$]$^+$. Reproduced with permission from [90].

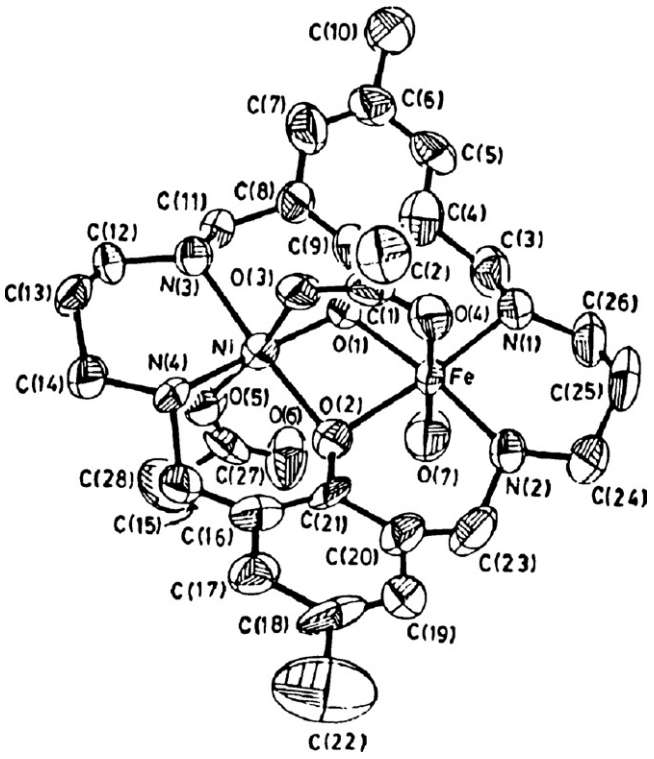


**Fig. 22.** X-ray structure of the complex cation [FeNi(μ-mac)(μ-OAc)(OAc)]$^+$. Reproduced with permission from [91].

A single $Fe^{II}Mn^{II}$ complex has been described by Que et al. using the tetrapyridyl ligand H-bpmp [90]. The compound has been structurally characterized (Fig. 21) but the two ions could not be precisely located owing to their similar ionic radii (Table 1). Its magnetic and EPR properties were investigated. As expected, the two ions were weakly antiferromagnetically coupled ($-2J = 4$–$8\ cm^{-1}$) and this magnetic exchange interaction is of the same order of magnitude as the zero-field splitting of the ferrous ion ($|D| = 5$–$7\ cm^{-1}$).

This complex was thoroughly studied by NMR. Indeed, owing to the short electronic relaxation time of the $Fe^{II}$ ion, it exhibits sharp resonances over a 210 ppm range that could be fully assigned [90,98].

Finally, a related $Fe^{III}Mn^{II}$ complex was isolated with a diphenol macrocyclic ligand (Scheme 3) by Nag et al. [91]. This complex is isostructural with the $Fe^{III}Ni^{II}$ derivative whose X-ray structure is depicted in Fig. 22. The rough planarity that is enforced by the macrocyclic ligand causes a significant reduction in the antiferromagnetic exchange interaction ($-2J = 4\ cm^{-1}$). This lowering can be attributed to a decrease in the Fe–O–Mn bridge angle from ca. 115° in the acyclic complexes [88,92] to ca. 90° in the macrocyclic one.

### 6.3. Summary and future work

This brief summary has stressed the paucity of FeMn complexes described in the literature and in particular as potential models of the enzymes active site. Moreover most studies have focused on the physical properties of the systems and no redox reactivity data are available yet.

## 7. Conclusions

This review has emphasized the emergence of a new class of enzymes with a FeMn active site. While enzymes possessing an heterodimetal active site were known for some time, their biological activities were restricted to hydrolytic reactions. The past few years

have seen the appearance of FeMn enzymes with redox activities: the one-electron oxidation to generate a radical has been described [12] and a two-electron substrate oxidation [86] may follow in the near future.

While the active center is new, the functions are already performed by diiron enzymes. This rises the question of the special need for a FeMn active site. The observation that these proteins are frequently encountered in pathogens and extremophiles has led to the interesting proposal that they constitute adaptation to the peculiar conditions faced by these organisms, in particular in terms of oxidative challenge [12,42].

Of course, changing the metal requirement of an enzyme will require the adaptation of the cofactor assembly machinery that may be more difficult to process and understand. These questions are generally overlooked when proteins are heterologously expressed and great care must be exercised "to ensure that the metalloenzymes being examined in molecular detail are physiologically relevant" [41].

## Note added in proof

While the article was under review, two important articles were published. Lubitz et al. [100] reported the X-ray structure and a detailed EPR study of a dimanganese ribonucleotide reductase from *Corynebacterium ammoniagenes*. An oxo/hydroxo bridged dimanganese center was located at ca. 7 Å from the tyrosine residue. A dipolar magnetic interaction of the dimanganese center with the tyrosyl radical splitted the EPR spectra of the latter into five lines. Extensive simulations of these spectra allowed to conclude that the dimanganese center was in the $Mn^{III}Mn^{III}$ oxidation state with the high spin $Mn^{III}$ ions weakly ferromagnetically coupled. A mechanism is proposed to explain activation of *Ca* RNR-R2 by hydrogen peroxide that is consistent with the earlier proposal of Stubbe [41]. Noodelman et al. [101] have performed extensive DFT analyses of structure, energetics, and spectroscopy of the Mn–Fe active site of *Chlamydia trachomatis* ribonucleotide reductase in four oxidation states $Fe^{II}Mn^{II}$, $Fe^{III}Mn^{III}$, $Fe^{III}Mn^{IV}$ and $Fe^{IV}Mn^{IV}$. The structural and the Mössbauer parameters of the $Fe^{III}Mn^{IV}$ active form could be reproduced by (μ-oxo)(μ-hydroxo) bridged models, in agreement with the proposal of Green et al. [51]. A thorough investigation of the location of the two metals led to propose that when the enzyme is metallated with $Mn^{II}$ in excess or prior to $Fe^{II}$ addition Mn is positioned in the site further from Phe127.

## Acknowledgements

Dr G. Blondin and Dr V. Duarte are gratefully acknowledged for critical reading of the manuscript.

## References

[1] K.J. Waldron, J.C. Rutherford, D. Ford, N.J. Robinson, Nature 460 (2009) 823.
[2] C. Andreini, I. Bertini, A. Rosato, Acc. Chem. Res. 42 (2009) 1471.
[3] Z. Ma, F.E. Jacobsen, D.P. Giedroc, Chem. Rev. 109 (2009) 4644.
[4] A. Changela, K. Chen, Y. Xue, J. Holschen, C.E. Outten, T.V. O'Halloran, A. Mondragon, Science 301 (2003) 1383.
[5] J.P. Emerson, E.G. Kovaleva, E.R. Farquhar, J.D. Lipscomb, L. Que, Proc. Natl. Acad. Sci. U.S.A. 105 (2008) 7347.
[6] A.F. Miller, Acc. Chem. Res. 41 (2008) 501.
[7] M. Merkx, D.A. Kopp, M.H. Sazinsky, J.L. Blazyk, J. Muller, S.J. Lippard, Angew. Chem. Int. Ed. 40 (2001) 2782.
[8] M.H. Sazinsky, S.J. Lippard, Acc. Chem. Res. 39 (2006) 558.
[9] A.J. Wu, J.E. Penner-Hahn, V.L. Pecoraro, Chem. Rev. 104 (2004) 903.
[10] D.W. Christianson, Acc. Chem. Res. 38 (2005) 191.
[11] G. Schenk, C.L. Boutchard, L.E. Carrington, C.J. Noble, B. Moubaraki, K.S. Murray, J. de Jersey, G.R. Hanson, S. Hamilton, J. Biol. Chem. 276 (2001) 19084.
[12] W. Jiang, D. Yun, L. Saleh, E.W. Barr, G. Xing, L.M. Hoffart, M.A. Maslak, C. Krebs, J.M. Bollinger, Science 316 (2007) 1188.
[13] C. Krebs, M.L. Matthews, W. Jiang, J.M. Bollinger, Biochemistry 46 (2007) 10413.
[14] Y.S. Choi, H.J. Zhang, J.S. Brunzelle, S.K. Nair, H.M. Zhao, Proc. Natl. Acad. Sci. U.S.A. 105 (2008) 6858.
[15] N. Sträter, W.N. Lipscomb, T. Klabunde, B. Krebs, Angew. Chem. Int. Ed. 35 (1996) 2024.
[16] N. Mitic, S.J. Smith, A. Neves, L.W. Guddat, L.R. Gahan, G. Schenk, Chem. Rev. 106 (2006) 3338.
[17] M.B. Twitchett, G. Schenk, M.A.S. Aquino, D.T.Y. Yiu, T.C. Lau, A.G. Sykes, Inorg. Chem. 41 (2002) 5787.
[18] J. Uppenberg, F. Lindqvist, C. Svensson, B. Ek-Rylander, G. Andersson, J. Mol. Biol. 290 (1999) 201.
[19] N. Sträter, T. Klabunde, P. Tucker, H. Witzel, B. Krebs, Science 268 (1995) 1489.
[20] G. Schenk, L.R. Gahan, L.E. Carrington, N. Mitic, M. Valizadeh, S.E. Hamilton, J. de Jersey, L.W. Guddat, Proc. Natl. Acad. Sci. U.S.A. 102 (2005) 273.
[21] G. Schenk, Y.B. Ge, L.E. Carrington, C.J. Wynne, I.R. Searle, B.J. Carroll, S. Hamilton, J. de Jersey, Arch. Biochem. Biophys. 370 (1999) 183.
[22] T. Waratrujiwong, B. Krebs, F. Spener, P. Visoottiviseth, FEBS J. 273 (2006) 1649.
[23] M. Olczak, J. Ciuraszkiewicz, H. Wojtowicz, D. Maszczak, T. Olczak, FEBS Lett. 583 (2009) 3280.
[24] W.L. DeLano, The PyMOL Molecular Graphics System, DeLano Scientific LLC, Palo Alto, CA, USA, 2002, http://www.pymol.org.
[25] K. Koizumi, K. Yamaguchi, H. Nakamura, Y. Takano, J. Phys. Chem. A 113 (2009) 5099.
[26] S. Gehring, P. Fleischhauer, M. Behlendorf, M. Huber, J. Lorosch, W. Haase, M. Dietrich, H. Witzel, R. Locke, B. Krebs, Inorg. Chim. Acta 252 (1996) 13.
[27] E.P. Day, S.S. David, J. Peterson, W.R. Dunham, J.J. Bonvoisin, R.H. Sands, J.L. Que, J. Biol. Chem. 263 (1988) 15561.
[28] J.H. Rodriguez, H.N. Ok, Y.M. Xia, P.G. Debrunner, B.E. Hinrichs, T. Meyer, N.H. Packard, J. Phys. Chem. 100 (1996) 6849.
[29] Y.S. Yang, J.M. McCormick, E.I. Solomon, J. Am. Chem. Soc. 119 (1997) 11832.
[30] R.S. Cox, G. Schenk, N. Mitic, L.R. Gahan, A.C. Hengge, J. Am. Chem. Soc. 129 (2007) 9550.
[31] J. Stubbe, D.G. Nocera, C.S. Yee, M.C.Y. Chang, Chem. Rev. 103 (2003) 2167.
[32] P. Nordlund, P. Reichard, Annu. Rev. Biochem. 75 (2006) 681.
[33] J.M. Bollinger, D.E. Edmondson, B.H. Huynh, J. Filley, J.R. Norton, J. Stubbe, Science 253 (1991) 292.
[34] B.E. Sturgeon, D. Burdi, S.X. Chen, B.H. Huynh, D.E. Edmondson, J. Stubbe, B.M. Hoffman, J. Am. Chem. Soc. 118 (1996) 7551.
[35] P. Nordlund, B.M. Sjoberg, H. Eklund, Nature 345 (1990) 593.
[36] D.T. Logan, X.D. Su, A. Aberg, K. Regnstrom, J. Hajdu, H. Eklund, P. Nordlund, Structure 4 (1996) 1053.
[37] A.C. Rosenzweig, C.A. Frederick, S.J. Lippard, P. Nordlund, Nature 366 (1993) 537.
[38] A.C. Rosenzweig, P. Nordlund, P.M. Takahara, C.A. Frederick, S.J. Lippard, Chem. Biol. 2 (1995) 409.
[39] A. Willing, H. Follmann, G. Auling, Eur. J. Biochem. 170 (1988) 603.
[40] Y. Huque, F. Fieschi, E. Torrents, I. Gibert, R. Eliasson, P. Reichard, M. Sahlin, B.-M. Sjöberg, J. Biol. Chem. 275 (2000) 25365.
[41] J. Cotruvo Jr., J. Stubbe, Biochemistry 49 (2010) 1297.
[42] M. Högbom, P. Stenmark, N. Voevodskaya, G. McClarty, A. Gräslund, P. Nordlund, Science 305 (2004) 245.
[43] C. Roshick, E.R. Iliffe-Lee, G. McClarty, J. Biol. Chem. 275 (2000) 38111.
[44] S. Pötsch, F. Lendzian, R. Ingemarson, A. Hornberg, L. Thelander, W. Lubitz, G. Lassmann, A. Gräslund, J. Biol. Chem. 274 (1999) 17696.
[45] N. Voevodskaya, M. Galander, M. Högbom, P. Stenmark, G. McClarty, A. Gräslund, F. Lendzian, Biochim. Biophys. Acta-Proteins Proteomics 1774 (2007) 1254.
[46] D. Yun, C. Krebs, G.P. Gupta, D.F. Iwig, B.H. Huynh, J.M. Bollinger, Biochemistry 41 (2002) 981.
[47] N. Voevodskaya, F. Lendzian, A. Gräslund, Biochem. Biophys. Res. Commun. 330 (2005) 1213.
[48] N. Voevodskaya, A.J. Narvaez, V. Domkin, E. Torrents, L. Thelander, A. Gräslund, Proc. Natl. Acad. Sci. U.S.A. 103 (2006) 9850.
[49] N. Voevodskaya, F. Lendzian, A. Ehrenberg, A. Gräslund, FEBS Lett. 581 (2007) 3351.
[50] W. Jiang, J.M. Bollinger, C. Krebs, J. Am. Chem. Soc. 129 (2007) 7504.
[51] J.M. Younker, C.M. Krest, W. Jiang, C. Krebs, J.M. Bollinger, M.T. Green, J. Am. Chem. Soc. 130 (2008) 15022.
[52] H. Zheng, Y. Zang, Y. Dong, V. Young, L. Que Jr., J. Am. Chem. Soc. 121 (1999) 2226.
[53] H.-F. Hsu, Y. Dong, L. Shu, V. Young, L. Que Jr., J. Am. Chem. Soc. 121 (1999) 5230.
[54] L. Saleh, C. Krebs, B.A. Ley, S. Naik, B.H. Huynh, J.J.M. Bollinger, Biochemistry 43 (2004) 5953.
[55] M. Shanmugam, P.E. Doan, N.S. Lees, J. Stubbe, B.M. Hoffman, J. Am. Chem. Soc. 131 (2009) 3370.
[56] D. Hristova, C.H. Wu, W. Jiang, C. Krebs, J. Stubbe, Biochemistry 47 (2008) 3989.
[57] J.M. Bollinger, W. Jiang, M.T. Green, C. Krebs, Curr. Opin. Struct. Biol. 18 (2008) 650.
[58] W. Jiang, D. Yun, L. Saleh, J.M. Bollinger, C. Krebs, Biochemistry 47 (2008) 13736.
[59] N. Voevodskaya, F. Lendzian, O. Sanganas, A. Grundmeier, A. Gräslund, M. Haumann, J. Biol. Chem. 284 (2009) 4555.
[60] N. Mitic, M.D. Clay, L. Saleh, J. Bollinger, J.M.E. Solomon, J. Am. Chem. Soc. 129 (1999) 9049.

[61] W. Jiang, L.M. Hoffart, C. Krebs, J.M. Bollinger, Biochemistry 46 (2007) 8709.
[62] W. Jiang, J.J. Xie, H. Norgaard, J.M. Bollinger, C. Krebs, Biochemistry 47 (2008) 4477.
[63] Y.S. Yang, J. Baldwin, B.A. Ley, J.M. Bollinger, E.I. Solomon, J. Am. Chem. Soc. 122 (2000) 8495.
[64] B.S. Pierce, T.E. Elgren, M.P. Hendrich, J. Am. Chem. Soc. 125 (2003) 8748.
[65] B.S. Pierce, M.P. Hendrich, J. Am. Chem. Soc. 127 (2005) 3613.
[66] M. Fontecave, Cell. Mol. Life Sci. 54 (1998) 684.
[67] A. Anjem, S. Varghese, J.A. Imlay, Mol. Microbiol. 72 (2009) 844.
[68] K. Roos, P. Siegbahn, Biochemistry 48 (2009) 1878.
[69] W. Jiang, L. Saleh, E.W. Barr, J.J. Xie, M.M. Gardner, C. Krebs, J.M. Bollinger, Biochemistry 47 (2008) 8477.
[70] W. Jiang, J. Xie, P.T. Varano, C. Krebs, J.J.M. Bollinger, Biochemistry 49 (2010) 5340.
[71] J. He, C. Hertweck, Chem. Biol. 10 (2003) 1225.
[72] J. He, C. Hertweck, J. Am. Chem. Soc. 126 (2004) 3694.
[73] R. Winkler, C. Hertweck, Angew. Chem. Int. Ed. 44 (2005) 4083.
[74] M. Simurdiak, J. Lee, H.M. Zhao, Chembiochem 7 (2006) 1169.
[75] G. Zocher, R. Winkler, C. Hertweck, G.E. Schulz, J. Mol. Biol. 373 (2007) 65.
[76] R. Winkler, G. Zocher, I. Richter, T. Friedrich, G.E. Schulz, C. Hertweck, Angew. Chem. Int. Ed. 46 (2007) 8605.
[77] C.R. Samples, T. Howard, F.M. Raushel, V.J. DeRose, Biochemistry 44 (2005) 11005.
[78] M. Zheng, S.V. Khangulov, G.C. Dismukes, V.V. Barynin, Inorg. Chem. 33 (1994) 382.
[79] R. Rardin, W. Tolman, S. Lippard, New J. Chem. 15 (1991) 417.
[80] M.P. Hendrich, E. Munck, B.G. Fox, J.D. Lipscomb, J. Am. Chem. Soc. 112 (1990) 5861.
[81] V.K. Korboukh, N. Li, E.W. Barr, J.M. Bollinger, C. Krebs, J. Am. Chem. Soc. 131 (2009) 13608.
[82] J.M. Bollinger, C. Krebs, A. Vicol, S.X. Chen, B.A. Ley, D.E. Edmondson, B.H. Huynh, J. Am. Chem. Soc. 120 (1998) 1094.
[83] K.E. Liu, D.L. Wang, B.H. Huynh, D.E. Edmondson, A. Salifoglou, S.J. Lippard, J. Am. Chem. Soc. 116 (1994) 7465.
[84] L.J. Murray, S.G. Naik, D.O. Ortillo, R. Garcia-Serres, J.K. Lee, B.H. Huynh, S.J. Lippard, J. Am. Chem. Soc. 129 (2007) 14500.
[85] C.S. Andersson, M. Högbom, Proc. Natl. Acad. Sci. U.S.A. 106 (2009) 5633.
[86] M. Högbom, J. Biol. Inorg. Chem. 15 (2009) 339.
[87] U. Bossek, T. Weyhermuller, K. Wieghardt, J. Bonvoisin, J.J. Girerd, J. Chem. Soc. Chem. Commun. (1989) 633.
[88] R.M. Buchanan, M.S. Mashuta, J.F. Richardson, K.J. Oberhausen, D.N. Hendrickson, R.J. Webb, M.A. Nanny, Inorg. Chem. 29 (1990) 1299.
[89] R. Hotzelmann, K. Wieghardt, U. Florke, H.J. Haupt, D.C. Weatherburn, J. Bonvoisin, G. Blondin, J.J. Girerd, J. Am. Chem. Soc. 114 (1992) 1681.
[90] T.R. Holman, Z.G. Wang, M.P. Hendrich, L. Que, Inorg. Chem. 34 (1995) 134.
[91] S.K. Dutta, R. Werner, U. Florke, S. Mohanta, K.K. Nanda, W. Haase, K. Nag, Inorg. Chem. 35 (1996) 2292.
[92] P. Karsten, A. Neves, A.J. Bortoluzzi, M. Lanznaster, V. Drago, Inorg. Chem. 41 (2002) 4624.
[93] S. Mukherjee, T. Weyhermuller, E. Bothe, K. Wieghardt, P. Chaudhuri, Dalton Trans. (2004) 3842.
[94] S. Ross, T. Weyhermuller, E. Bill, E. Bothe, U. Florke, K. Wieghardt, P. Chaudhuri, Eur. J. Inorg. Chem. (2004) 984.
[95] The cyano-bridged compounds of Prussian Blue type are out of the scope of the present review.
[96] X.Y. Kuang, K.W. Zhou, Chem. Phys. Lett. 365 (2002) 122.
[97] A.S. Borovik, L. Que, V. Papaefthymiou, E. Munck, L.F. Taylor, O.P. Anderson, J. Am. Chem. Soc. 110 (1988) 1986.
[98] Z.G. Wang, T.R. Holman, L. Que, Magn. Res. Chem. 31 (1993) S78.
[99] E. Bernard, W. Moneta, J. Laugier, S. Chardon-Noblat, A. Deronzier, J.-P. Tuchagues, J.-M. Latour, Angew. Chem. Int. Ed. 33 (1994) 887.
[100] Lubitz, et al., J. Am. Chem. Soc. 132 (2010) 11197.
[101] Noodelman, et al., Inorg. Chem. 49 (2010) 7266.